Solar Irradiance Variability and Climate

Sami K. Solanki,[1,2] Natalie A. Krivova,[1] and Joanna D. Haigh[3]

[1]Max-Planck-Institut für Sonnensystemforschung, 37191 Katlenburg-Lindau, Germany; email: solanki@mps.mpg.de, natalie@mps.mpg.de

[2]School of Space Research, Kyung Hee University, Yongin, Gyeonggi 446-701, Korea

[3]Imperial College, London SW7 2AZ, United Kingdom; email: j.haigh@imperial.ac.uk

Annu. Rev. Astron. Astrophys. 2013. 51:311–51

First published online as a Review in Advance on June 26, 2013

The *Annual Review of Astronomy and Astrophysics* is online at astro.annualreviews.org

This article's doi: 10.1146/annurev-astro-082812-141007

Keywords

Sun: magnetic fields, Sun: photosphere, Sun: variability, Sun: irradiance, Sun: activity, Earth: climate, Earth: global change, Earth: stratosphere, Earth: atmospheric chemistry

Abstract

The brightness of the Sun varies on all timescales on which it has been observed, and there is increasing evidence that this has an influence on climate. The amplitudes of such variations depend on the wavelength and possibly the timescale. Although many aspects of this variability are well established, the exact magnitude of secular variations (going beyond a solar cycle) and the spectral dependence of variations are under discussion. The main drivers of solar variability are thought to be magnetic features at the solar surface. The climate response can be, on a global scale, largely accounted for by simple energetic considerations, but understanding the regional climate effects is more difficult. Promising mechanisms for such a driving have been identified, including through the influence of UV irradiance on the stratosphere and dynamical coupling to the surface. Here, we provide an overview of the current state of our knowledge, as well as of the main open questions.

1. INTRODUCTION

total solar irradiance (TSI): the total power from the Sun impinging on a unit area perpendicular to the Sun's rays at 1 AU

SSI: spectral solar irradiance

The Sun is a very special star. Not only is it a boon to astronomers in that it allows us to start resolving spatial scales at which universal physical processes take place that act in other astronomical objects but it is the only star that directly influences Earth and, thus, our lives.

Of the many ways in which the Sun affects Earth, the most obvious is by its radiation. The approximately 1,361 W m^{-2} received from the present day Sun at 1 AU (the total solar irradiance, see below) are responsible for keeping Earth from cooling off to temperatures that are too low for sustaining human life. The composition, structure, and dynamics of Earth's atmosphere also play a very fundamental part by making efficient use (through the greenhouse effect) of the energy input from the Sun.

The total solar irradiance, or TSI, is defined as the total power from the Sun impinging on a unit area (perpendicular to the Sun's rays) at 1 AU (given in units of Watts per meter squared). The TSI is the wavelength integral over the spectral solar irradiance, or SSI (given in Watts per meter squared per nanometer).

Under normal circumstances, the Sun is the only serious external source of energy to Earth. Any variability of the Sun's radiative output thus has the potential of affecting our climate and, hence, the habitability of Earth. The important question is how strong this influence is and, in particular, how it compares with other mechanisms including the influence of man-made greenhouse gases. Although this has been debated for a long time, the debate is being held with increasing urgency due to the unusual global temperature rise we have seen in the course of the twentieth century and particularly during the past 3–4 decades. It is generally agreed that the recent warming is mainly driven by the release of greenhouse gases, foremost among them carbon dioxide, into Earth's atmosphere by the burning of fossil fuels (Solomon et al. 2007). However, determining the exact level of warming due to man-made greenhouse gases requires a good understanding of the natural causes of climate change. These natural causes are to be found partly in the climate system itself (which includes the oceans and the land surfaces) and partly arise from Earth's interior (by the release of aerosols and dust through volcanoes), but they also lie outside Earth, and these sources are, thus, astronomical in nature.

A variety of astronomical effects can influence Earth's climate. Thus the energetic radiation from a nearby supernova could adversely affect our atmosphere in a dramatic fashion (e.g., Svensmark 2012). Also, modulation of cosmic rays as the Sun passes into and out of spiral arms during its orbit around the Galaxy has been proposed to explain slow variations in climate taking place over hundreds of millions of years (Shaviv 2002).

However, the most obvious astronomical influence is due, directly or indirectly, to the Sun, which is the source of practically all external energy input into our climate system. The Sun's influence can follow three different paths: (*a*) variations in insolation through changes in the Sun's radiative output itself (direct influence); (*b*) modulations of the radiation reaching different hemispheres of Earth through changes in Earth's orbital parameters and in the obliquity of its rotation axis (indirect influence); and (*c*) the influence of the Sun's activity on Galactic cosmic rays (GCRs) proposed to affect cloud cover (e.g., Marsh & Svensmark 2000).

The first of these is generally considered to be the main cause of the solar contribution to global climate change and will be described in greater detail below. We need to distinguish between changes in TSI, i.e., in the energy input to the Earth system, and variations in SSI, particularly in UV irradiance, which can enhance the Sun's effect by impacting the chemistry in Earth's middle atmosphere.

The second path is now accepted as the prime cause of the pattern of ice ages and the interglacial warm periods that have dominated the longer term evolution of the climate over the past few

million years. The various parameters of Earth's orbital and rotational motion vary at periods of 23 kyr (precession), 41 kyr (obliquity), and 100 kyr (eccentricity) (e.g., Crucifix, Loutre & Berger 2006; Paillard 2001). The changes in Earth's orbit are so slow that they are unlikely to have contributed to the global warming over the past century.

The third potential path builds on the modulation of the flux of Galactic cosmic rays by solar magnetic activity. The Sun's open magnetic flux (i.e., the flux in the field lines reaching out into the heliosphere) and the solar wind impede the propagation of the charged GCRs into the inner Solar System, so that at times of high solar activity fewer cosmic rays reach Earth. Their connection with climate has been drawn by, e.g., Marsh & Svensmark (2000) from the correlation between the cosmic-ray flux and global cloud cover. However, this mechanism still has to establish itself. Thus the CLOUD experiment at CERN has so far returned only equivocal results on the effectiveness of cosmic rays in producing clouds (Kirkby et al. 2011).

In this review, we provide an overview of our knowledge of solar irradiance variability and of the response of Earth's climate to changes in solar irradiance. Consequently, the second and third mechanisms of the Sun's influence are not considered further here. A number of earlier reviews have also covered all or aspects of this topic. Overviews of solar irradiance variability have been given by Lean (1997), Fröhlich & Lean (2004), Solanki, Krivova & Wenzler (2005), Domingo et al. (2009), Lean & DeLand (2012), and Krivova & Solanki (2012). The solar activity variations underlying irradiance changes have been reviewed by Usoskin (2008), Hathaway (2010), Charbonneau (2010), and Usoskin, Solanki & Kovaltsov (2012). Solar irradiance together with the response of Earth's atmosphere have been covered by Haigh, Lockwood & Giampapa (2005), Haigh (2007), Gray et al. (2010), and Ermolli et al. (2013) [cf. the monograph edited by Pap et al. (2004)].

Here, we first discuss the measurements of solar irradiance variations, their causes and models aiming to reproduce the data (Section 2), followed by an overview of longer term evolution of solar activity and the associated evolution of solar irradiance (Section 3). In Section 4, we move to the response of Earth's atmosphere to solar irradiance variations, with conclusions being given in Section 5.

2. SHORT-TERM SOLAR IRRADIANCE VARIABILITY

2.1. Measurements of Total and Spectral Solar Irradiance

The measurement of solar irradiance with accuracy sufficiently high to detect and reliably follow the tiny, 0.1%, changes exhibited by the Sun was a remarkable achievement. In the meantime, missions such as COROT (*COnvection, ROtation and planetary Transits*; Baglin et al. 2002) and *Kepler* (Borucki et al. 2003) can detect similar levels of fluctuations on myriads of stars, but reliably measuring the variability of the Sun remains a particular challenge because of the immense brightness contrast of the Sun compared with other astronomical objects, so that maintaining photometric calibrations employing comparisons with many stars is difficult at best (although some instruments do employ this technique in the UV).

Many attempts to measure the so-called solar constant preceded the satellite measurements that finally revealed its variability. Presatellite measurements of the solar constant obtained absolute values ranging from 1,338 W m^{-2} to 1,428 W m^{-2} (see reviews by Fröhlich & Brusa 1981 and Smith & Gottlieb 1974). These measurements were too inaccurate to detect intrinsic changes in the solar brightness, even though their presence was suspected (e.g., Eddy 1976). Space-borne radiometers (e.g., Fröhlich 2006, Hickey et al. 1980, Willson & Hudson 1988) provide an almost uninterrupted record of TSI since November 1978 (see **Figure 1**). These instruments are accurate

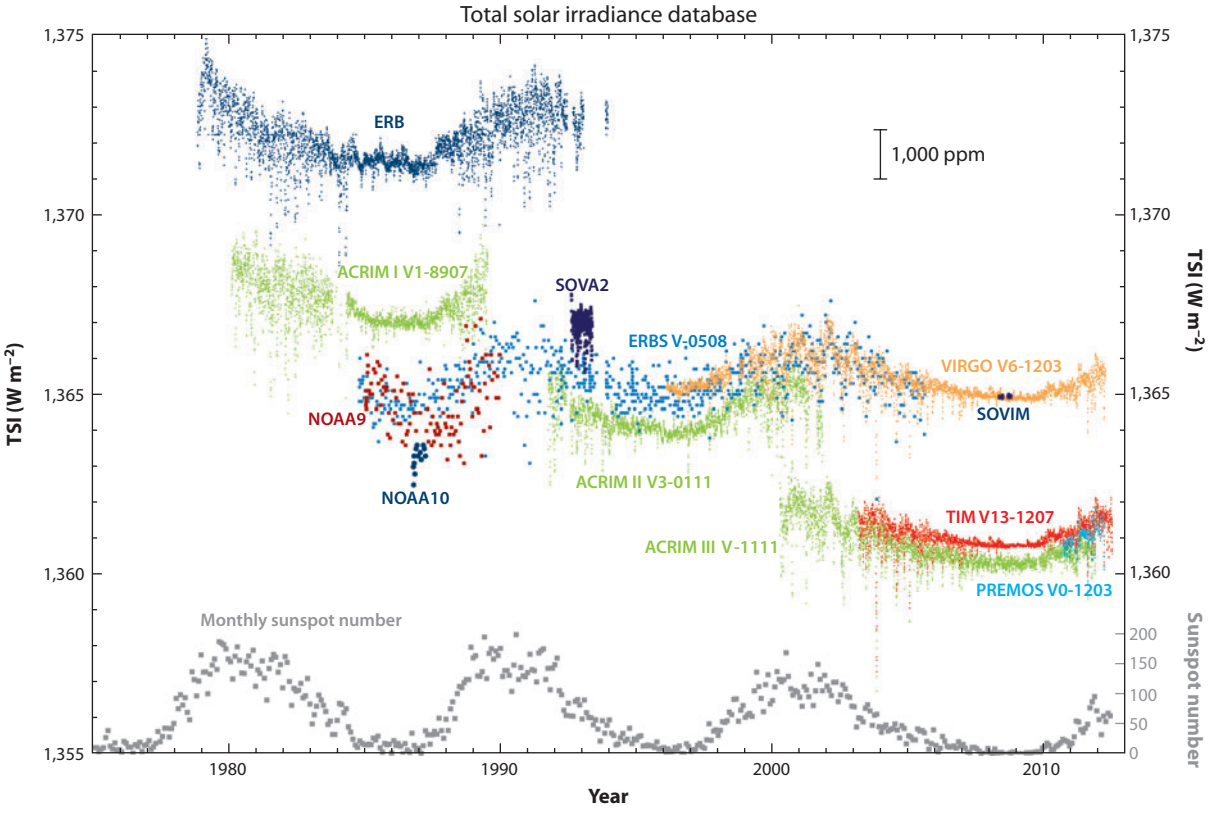

Figure 1

Space-borne total solar irradiance (TSI) measurements covering the period of 1978–2012 after the TRF (TSI Radiometer Facility) corrections. Individual records are shown in different colors, as labeled in the plot. The bottom part of the plot shows the monthly mean sunspot number. Courtesy of G. Kopp (**http://spot.colorado.edu/~koppg/TSI/**). Abbreviations: ACRIM, Active Cavity Radiometer Irradiance Monitor; ERB, Earth Radiation Budget instrument; ERBS, *Earth Radiation Budget Satellite*; NOAA, National Oceanic and Atmospheric Administration; PREMOS, Precision Monitor Sensor; SOVA, Solar Variability Experiment; SOVIM, Solar Variability and Irradiance Monitor; TIM, Total Irradiance Monitor; VIRGO, Variability of Solar Irradiance and Gravity Oscillations.

and stable enough to trace irradiance *variability* up to the solar cycle timescale, as revealed in **Figure 1** by the similarity of the curves recorded by different instruments. All the curves (with sufficient time resolution) show two striking features: a trend following the solar cycle, with the irradiance being higher during cycle phases with higher activity, and short (week-long) dips in irradiance that coincide with the passage of sunspots across the solar disk.

However, the radiometric accuracy of individual TSI measurements was generally poorer than the ~0.1% solar cycle change, as indicated by the scatter in absolute values in **Figure 1**. A discrepancy of roughly 5 W m^{-2}, or 0.35%, has been present between the values measured by instruments launched in the 1980s and 1990s and the Total Irradiance Monitor (TIM) on the *Solar Radiation and Climate Experiment* (SORCE) launched in 2003 (see **Figure 1**). This discrepancy appears to have been resolved thanks to recent tests with the TSI Radiometer Facility (TRF), which allows TSI instruments to be validated against a NIST (National Institute of Standards and Technology)-calibrated cryogenic radiometer at full solar power under vacuum conditions before launch. It has been used to calibrate the Precision Monitor Sensor (PREMOS) on *PICARD* (a satellite named

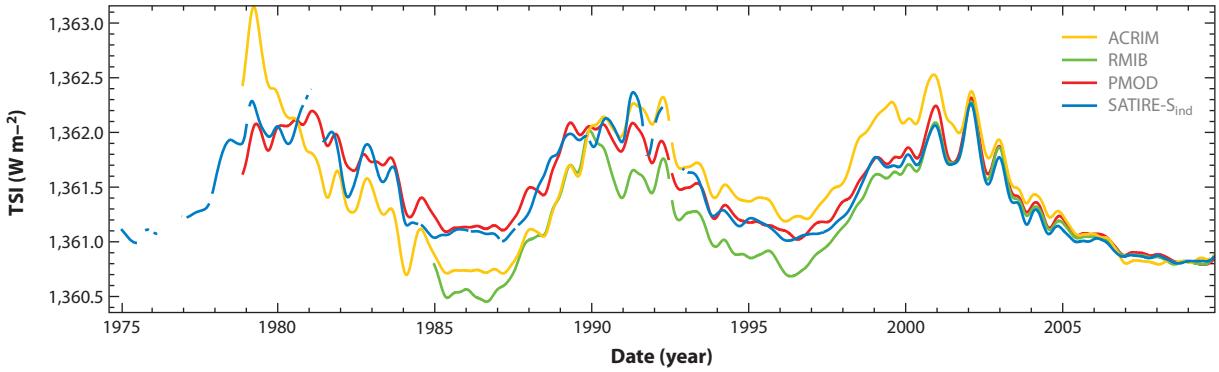

Figure 2

Comparison of the three smoothed total solar irradiance (TSI) composites (ACRIM, *yellow*; RMIB, *green;* and PMOD, *red*) as well as TSI reconstructed by the SATIRE-S (*blue*), all normalized to the SORCE/TIM at the minimum in December 2008. Gaps in the curves are gaps in the data longer than 27 days. Credit: Ball et al. (2012), reproduced with permission ©ESO. Abbreviations: ACRIM, Active Cavity Radiometer Irradiance Monitor; RMIB, Royal Meteorological Institute of Belgium; PMOD, Physikalisch-Meteorologisches Observatorium Davos; SATIRE-S, Spectral and Total Irradiance Reconstructions for the Satellite era; SORCE, *Solar Radiation and Climate Experiment*; TIM, Total Irradiance Monitor.

after the French astronomer Jean Picard), as well as ground-based representatives of the TIM on SORCE, the Variability of Solar Irradiance and Gravity Oscillations (VIRGO) instrument on the *Solar Heliospheric Observatory* (SoHO), and the Active Cavity Radiometer Irradiance Monitor (ACRIM) on the ACRIMSAT (*Active Cavity Radiometer Irradiance Monitor Satellite*; Fehlmann et al. 2012, Kopp & Lean 2011, Kopp et al. 2012). TRF-based tests and corrections brought PREMOS and ACRIM3 into close agreement, to within 0.05%, with TIM (Fehlmann et al. 2012, Kopp et al. 2012). Thus a TSI value of 1,360.8 $\pm$ 0.5 W m^{-2} is currently considered to best represent solar minimum conditions (Kopp et al. 2012).

The discrepancy in absolute values of individual TSI measurements makes it hard to assess irradiance changes on timescales longer than the solar cycle because individual radiometers rarely covered more than a single solar activity minimum. To trace long-term changes, individual irradiance measurements need to be adjusted to the same absolute scale, which is a nontrivial task due to instrumental degradation, sensitivity changes, and other problems. In particular, early sensitivity changes, when a radiometer starts being exposed to sunlight, need to be taken into account (e.g., Dewitte, Crommelynck & Joukoff 2004; Fröhlich 2006; Lee et al. 1995), but also sudden changes in calibration or noise-level, like the ones that occurred on the *Nimbus*-7 Earth Radiation Budget (ERB) instrument (Hoyt et al. 1992, Lee et al. 1995), can complicate a "cross-calibration" process.

Consequently, it is not surprising that three different composites have been produced, which are named after the instrument that they take as the basis or the institute at which the composite is produced: ACRIM (Willson 1997, Willson & Mordvinov 2003), RMIB (named after the Royal Meteorological Institute of Belgium, sometimes also called IRMB in the francophonic tradition; Dewitte et al. 2004) and PMOD (Physikalisch-Meteorologisches Observatorium Davos; Fröhlich 2006). These composites are plotted in **Figure 2** after imposing a temporal filtering to bring out the longer term changes. The composites agree in many respects, e.g., on short timescales, and they also share most of the features on longer timescales.

The most critical difference between them concerns their longer term trends, which become most clearly visible by comparing the TSI levels during activity minima, i.e., at times when different levels of TSI are easily distinguishable. Such long-term changes are particularly interesting in the

context of the global climate change as witnessed in the past century, which explains the debate that these differences in trend have sparked. The ACRIM composite shows an upward trend between the minima in 1986 and 1996, whereas TSI decreases from 1996 to 2008. In the RMIB composite, TSI increases from the minimum in 1996 to 2008. The PMOD TSI shows the opposite trend. The differences in the composites and their sources are described in more detail by Fröhlich (2006, 2012). Independent models assuming irradiance variability to be driven by the evolution of the surface magnetic field agree better with the PMOD long-term trend (see Section 2.3).

Space-based observations of SSI also started in 1978 with the *Nimbus*-7 Solar Backscatter Ultraviolet (SBUV) radiometer (Cebula, DeLand & Schlesinger 1992), and until 2002 were almost exclusively limited to the UV range below 400 nm. They were reviewed by DeLand & Cebula (2008, 2012). DeLand & Cebula (2008) have also collected the earlier UV data and combined them into a single record. The cross calibration of individual data sets and construction of a self-consistent composite is, however, in this case even more challenging than the cross calibration for the TSI.

First observations in the visible and IR were sporadic [e.g., by the SOLar SPECtrum, SOLSPEC, and SOSP instruments flown on space shuttles or on the EUropean REtrieval CArrier platform (Thuillier et al. 2003, 2004; see also overviews by Thuillier et al. 2009 and Ermolli et al. 2013)]. These early measurements were used to produce ATLAS (Atmospheric Laboratory for Applications and Science) solar reference spectra ATLAS1 (March 1992) and ATLAS3 (November 1994) (Thuillier et al. 2004). More recent solar reference spectra were produced within the Whole Heliosphere Interval (WHI) international campaign during three relatively quiet periods in March–April 2008 (Woods et al. 2009). One of these spectra, produced during the most quiet period (the WHI quiet Sun reference spectrum), is shown in **Figure 3*a*** (on a logarithmic scale to allow for the differences in irradiance in the UV and the visible). The strong emission line is Lyα.

Assessment of the SSI variability is complicated and, until relatively recently, this was only possible in the UV range, mainly thanks to the two instruments on board the *Upper Atmosphere Research Satellite* (UARS): the Solar Stellar Irradiance Comparison Experiment (SOLSTICE; Rottman, Woods & Sparn 1993) and the Solar Ultraviolet Spectral Irradiance Monitor (SUSIM; Brueckner et al. 1993). In the UV below about 250 nm, long-term instrumental uncertainties of SOLSTICE and SUSIM were smaller than the solar variability (e.g., Woods et al. 1996). **Figure 3*b*** illustrates the relative difference in the irradiance spectrum between activity maximum and minimum. (Note that SORCE was launched in 2003, and SIM data are only available since April 2004. Thus using the SORCE data, SSI variability can be estimated for only over less than half a cycle.) Clearly, the irradiance variability is a strong function of wavelength and increases very rapidly toward shorter wavelengths in the UV (note the logarithmic scale). In spite of differences in detail, all data sets show a qualitatively similar behavior in the UV, illustrated by the red and blue curves. Quantitatively, there are differences of up to nearly an order of magnitude, which do not appear so striking due to the logarithmic scaling. They are discussed below.

Results from the SORCE launched in 2003 sprang a surprise. The SORCE carries two instruments—the SOLSTICE (an analog of UARS/SOLSTICE; Snow et al. 2005) and the Spectral Irradiance Monitor (SIM) (Harder et al. 2005)—that observe SSI over a broad spectral range from Lyα to 2,400 nm. Between 2003 and 2008, i.e., over the declining phase of cycle 23, SIM displayed an anticyclic behavior in the visible band, i.e., the irradiance at most visible and IR wavelengths is lower at higher activity levels than during quiet times (Harder et al. 2009). This is indicated by the dotted blue line in **Figure 3**. These values would be negative (which cannot be directly represented on a logarithmic scale). This antiphase behavior to the TSI is largely compensated by the enhanced in-phase UV variability between 200 and 400 nm compared with previous measurements. Thus the estimated contribution of the 200–400 nm spectral range to the

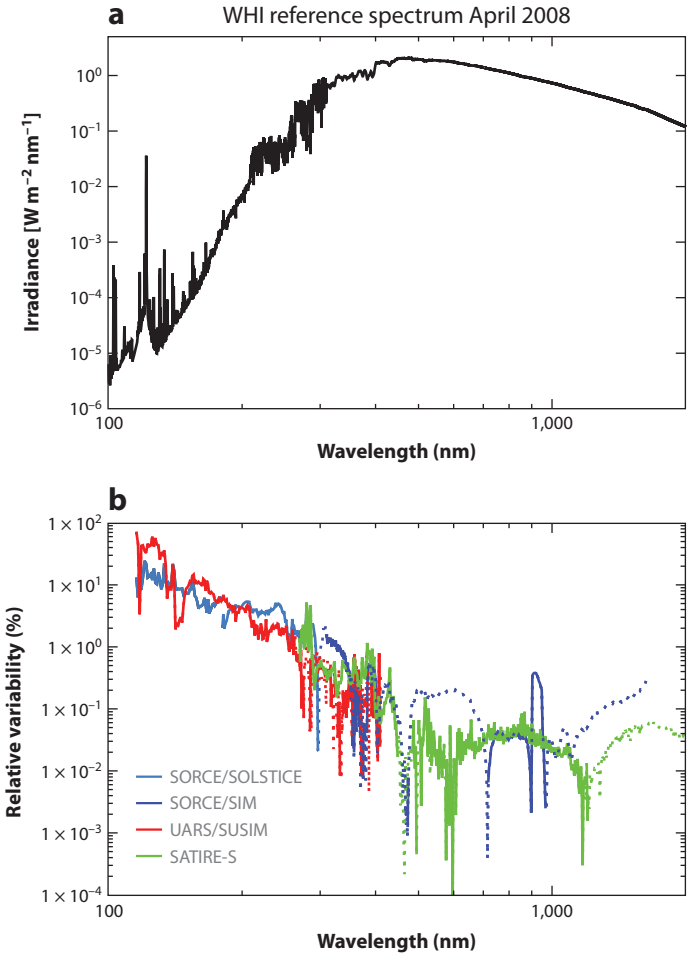

Figure 3

(*a*) Reference solar spectrum recorded in April 2008 (Woods et al. 2009). (*b*) Relative spectral solar irradiance variability as observed by the UARS/SUSIM (*red*; Floyd et al. 2003) between the maximum of cycle 23 (March 2000) and the preceding minimum (May 1996), as well as by the SORCE/SOLSTICE (*light blue*; Snow et al. 2005) and the SORCE/SIM (*dark blue*; Harder et al. 2009) between April 2004 and December 2008. Also shown is the variability between 2000 and 1996 predicted by the SATIRE-S model (*green*; Krivova et al. 2009, Krivova, Solanki & Unruh 2011). For each period, averages over one month are used. Negative values are indicated by dotted segments. Abbreviations: SATIRE-S, Spectral and Total Irradiance Reconstruction for the Satellite era; SIM, Spectral Irradiance Monitor; SOLSTICE, Solar Stellar Irradiance Comparison Experiment; SORCE, *Solar Radiation and Climate Experiment;* SUSIM, Solar Ultraviolet Spectral Irradiance Monitor; UARS, *Upper Atmosphere Research Satellite*; WHI, Whole Heliosphere Interval.

TSI decrease from 2004 to 2008 was about 180% (Harder et al. 2009), compared with 20–60% based on earlier measurements (Krivova, Solanki & Floyd 2006; Lean et al. 1997; Morrill, Floyd & McMullin 2011; Thuillier et al. 2004).

At the same time, the short-term (rotational) variability measured by SORCE/SOLSTICE and SORCE/SIM agrees with previous results very well. Because shorter timescales are significantly less affected by instrumental effects, DeLand & Cebula (2012) conclude that undercorrection of response changes for the SORCE instruments is the most probable reason for the discrepancies.

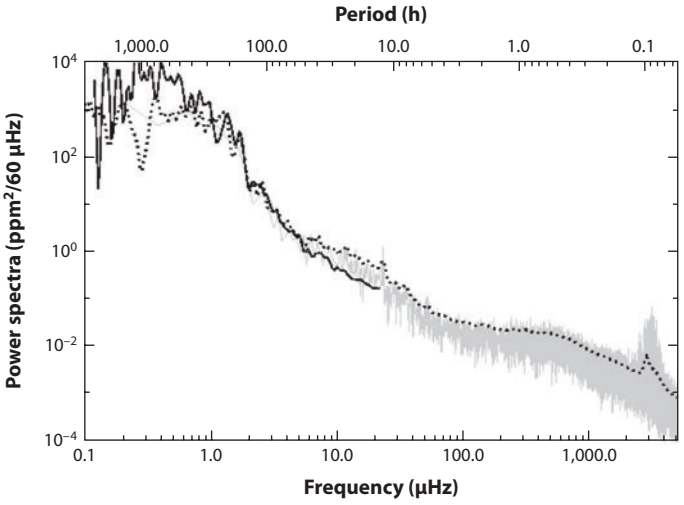

Figure 4

Power spectrum of total solar irradiance. The different curves show Fourier (*gray line*) and global wavelet (*black dotted line*) power spectra of the VIRGO data set for the year 2002 sampled at a 1-min cadence (Fröhlich et al. 1995). The black solid line shows the global wavelet spectrum of the SORCE/TIM data (Kopp, Lawrence & Rottman 2005) for the year 2003 sampled every 6 h. Credit: Seleznyov, Solanki & Krivova (2011), reproduced with permission ©ESO. Abbreviations: SORCE, *Solar Radiation and Climate Experiment*; TIM, Total Irradiance Monitor; VIRGO, Variability of Solar Irradiance and Gravity Oscillations instrument.

The importance of getting the correct spectral dependence of the irradiance variations lies in the fact that the UV irradiance influences atmospheric chemistry more strongly than that of the visible, although the visible cannot be neglected (see Section 4).

2.2. Physical Causes of Irradiance Variations

There are a variety of causes of solar irradiance variations, and each acts on particular timescales. This is illustrated in **Figure 4** for a limited set of timescales by plotting the power spectrum of TSI for periods from about 1 min to 1 year (Seleznyov, Solanki & Krivova 2011). The power drops very roughly as a power law from long to short timescales. These variations are driven by a range of sources. Thus solar oscillations, the *p*-modes, are responsible for the group of peaks centered around 5 min (3 mHz), the evolution of granules produces the plateau between 50 and 500 μHz (i.e., on periods of minutes to hours), whereas the rotational modulation of TSI by the passage of sunspots and faculae over the solar disc leads to the increase in power between 0.4 and 50 μHz (i.e., periods of between about 5 and 5,000 hours). The solar rotation period itself does not display a significant peak in this figure, however, owing to the combination of the limited lifetime of sunspots (most live only a few days or less) and the constant evolution of the brightness of the longer lived active regions, as well as the rather common occurrence of multiple active regions on the Sun at the same time.

From the solar rotation period to the 10–12-year solar cycle period, the growth, evolution, and decay of active regions, as well as the distribution of their remnant magnetic field over the solar surface provide the main contribution to the variability. This is strongly modulated by the activity cycle itself, which is a very strong contributor to irradiance variations. Beyond the solar cycle period, the difference in the strength of individual cycles as well as possible evolution of the

background field and other mechanisms (see Section 3) may lead to a secular change, which might be visible in the form of different TSI levels at the different minima. Over the thermal relaxation timescale of the convection zone of 10^5 years, the energy blocked by sunspots should be gradually released again (see below), whereas beyond 10^6 years the gradual brightening of the Sun due to the chemical evolution of its core should start to become noticeable in its TSI (e.g., Charbonnel et al. 1999; Mowlavi et al. 2012; Sackmann, Boothroyd & Kraemer 1993).

With the exception of the shortest and the longest timescales, the causes of irradiance variations listed above are associated more or less directly with the Sun's magnetic field mainly via the influence of magnetic fields on the thermal structure of the solar surface and atmosphere.

For irradiance variations of possible relevance to global climate change, the magnetic field is expected to be the main driving force. Of importance is the magnetic field at the solar surface and, in the lower solar atmosphere, mainly the photosphere (see, e.g., Solanki & Unruh 1998). In these layers the magnetic field is thought to be concentrated into strong field features (having an average field strength of roughly a kilogauss in the mid-photosphere; Solanki et al. 1999) whose simplest description is by magnetic flux tubes (see Solanki 1993 for a review), although their real structure is more complicated (e.g., Rempel et al. 2009, Stein 2012, Vögler et al. 2005). Another, more chaotic component of the magnetic field is present as well (see de Wijn et al. 2009 for a review). It is still unclear whether this turbulent field component really contributes to irradiance variations, so we restrict ourselves to the concentrated fields, which range in cross-section size between structures well below 100 km in diameter to sunspots that often have dimensions of multiple tens of megameters.

Sunspots, forming the hearts of active regions, clearly are dark (see Rempel & Schlichenmaier 2011, Solanki 2003 for reviews), whereas the small magnetic elements that populate (and form) the faculae in active regions and the network elsewhere on the Sun (and are even found in the internetwork of the quiet Sun; Lagg et al. 2010, Sánchez Almeida et al. 2004) are bright, particularly near the limb and at wavelengths formed above the solar surface. Such wavelengths include the Fraunhofer g-band (Berger et al. 1995, Muller & Roudier 1984), the CN bandhead (Sheeley 1969, Zakharov et al. 2007), the cores of strong spectral lines (e.g., Skumanich, Smythe & Frazier 1975), and the UV (Riethmüller et al. 2010).

The darkness of sunspots is due to the blocking of heat flowing from below by the kilogauss magnetic field, which is strong enough to largely quench overturning convection (Rempel & Schlichenmaier 2011). Forms of magnetoconvection do take place, maintaining the penumbra's (and to some extent also the umbra's) brightness (e.g., Joshi et al. 2011, Rempel et al. 2009, Scharmer et al. 2011, Schüssler & Vögler 2006).

The magnetic elements have a nearly equally strong field (as sunspots averaged over their cross section), so that the convective energy flux from below is greatly reduced in their interiors. This is indicated by the different lengths of the vertical red arrows in **Figure 5**. This figure displays the vertical cross section of an intense slender flux tube. Another feature that can be seen in the figure is the depression of the optical depth unity surface (*heavy blue line*) in the flux tube's interior. Hence, for depths up to ΔZ below the solar surface in the quiet Sun, the walls of the flux tube allow radiation to escape into space. This radiation heats up the interior of the tube. Furthermore, photons from these hot walls (which are windows into the hot interior of the Sun) can be directly observed, best when the magnetic element is located at some distance away from the solar disc center (Carlsson et al. 2004, Keller et al. 2004, Spruit 1976).

In addition to this radiative heating, the magnetic elements are shaken and squeezed by the turbulently convective gas in their surroundings. This causes the excitation of different wave modes within them (Musielak & Ulmschneider 2003). This mechanical transfer of energy from

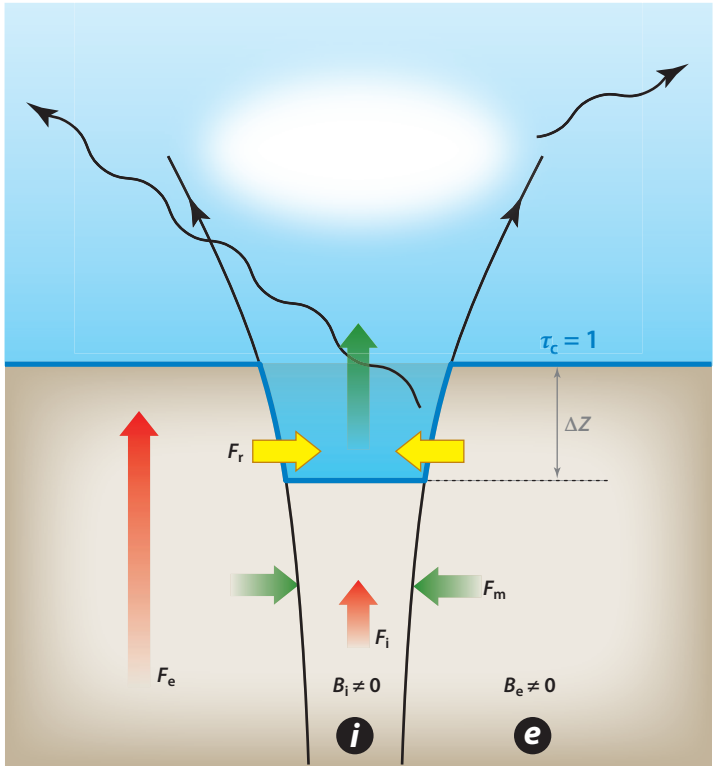

Figure 5

Sketch of the vertical cross section through a slender magnetic flux tube. The arrows illustrate the various forms of energy transfer. Red arrows represent vertical convective and radiative energy flux below the solar surface inside the flux tube (subscript i) and in the external medium (subscript e). Yellow arrows represent horizontal influx of radiation through the walls of the flux tube (the *blue thick lines* outline the optical depth unity, $\tau_c = 1$, surface, as seen from above). ΔZ represents the Wilson depression. Green arrows represent mechanical energy flux. The cloud sketches the hot chromospheric layers of the magnetic feature [roughly following a sketch by Zwaan (1978)].

the surroundings into the tubes is represented in **Figure 5** by the green horizontal arrows, whereas the upward transport of the mechanical energy by waves is indicated by the vertical green arrow.

In particular, the longitudinal tube waves steepen as they propagate upward, due to the drop in density, finally dissipating their energy at shocks in the chromosphere (e.g., Carlsson & Stein 1997; Fawzy, Cuntz & Rammacher 2012). Other forms of heating may also be taking place, but are not discussed further here. This leads to a heating of the upper photospheric and chromospheric layers of magnetic elements, which explains their excess brightness in the UV and in the cores of spectral lines (e.g., CaII H and K; see Rezaei et al. 2007, Schrijver et al. 1989). Whereas the radiation flowing in from the walls penetrates the small magnetic features completely, for features with horizontal dimensions greater than roughly 400 km the radiation cannot warm the inner parts and they remain cool and dark, cf. Grossmann-Doerth et al. (1994). The radiative properties of sunspots (and to a lesser extent the smaller, but still dark pores) and magnetic elements are responsible for most of the irradiance variations on timescales of days to the solar cycle and very likely also beyond that to centuries and millennia, as described in the following sections.

However, one important question remains: Why does the energy blocked by the magnetic field in sunspots not simply flow around them and appear as a surrounding bright ring? Such bright rings have been found (e.g., Rast et al. 2001, Waldmeier 1939), but prove to release only a few percent of the energy flux blocked by the enclosed sunspots. An explanation was provided by Spruit (1982a,b), who showed that the energy blocked by sunspots is redistributed in the solar convection zone due to the very high heat conductivity of the solar plasma (see Spruit 2000 for a review). Due to the very high heat capacity, the stored heat hardly changes the surface properties at all. This heat is gradually re-emitted over the Kelvin-Helmholtz timescale of the convection zone, which is approximately 10^5 years. In analogy, the excess radiation emitted by magnetic elements also comes from the convection zone's large heat reservoir. Consequently, one may consider magnetic elements as leaks in the solar surface because by dint of being evacuated they increase the solar surface area (see **Figure 5**).

Alternative explanations to the TSI variations on timescales of the solar cycle and longer have also been proposed, e.g., thermal shadows produced by horizontal magnetic flux in the solar interior (Kuhn et al. 1998) or long-period ($\approx$1 month) oscillations driven by the Coriolis force (r-modes; Wolff & Hickey 1987). As we shall see in the next subsection, the surface magnetic field leaves at most a few percent of the TSI variations on timescales up to the solar cycle to be explained by these or other such mechanisms. However, it cannot be ruled out that one of these mechanisms (or an as yet unknown one) may contribute significantly on longer timescales (e.g., Sofia & Li 2001).

2.3. Modeling of Total and Spectral Solar Irradiance

Models assuming that irradiance variations on timescales longer than roughly a day are caused by changes in the surface distribution of different magnetic features (see Section 2.2) turned out to be the most successful in explaining observed irradiance changes. The first models of this type (e.g., Foukal & Lean 1986; Oster, Schatten & Sofia 1982; Willson et al. 1981) were so-called proxy models, which combined proxies of solar surface magnetic features using regressions to match observed TSI changes. Proxies that have been used most frequently include the sunspot area and the photometric sunspot index (PSI) derived from it (a measure of sunspot darkening), as well as MgII, CaII, and F10.7 (solar radio flux at 10.7 cm) indices to describe facular brightening. The widely used MgII index is the ratio of the brightness in the cores of the MgII lines to their wings, making it relatively insensitive to instrumental degradation with time (Viereck et al. 2001). However, it is sensitive to the exact wavelength choice, which leads to uncertainties in the long-term trend in the composite MgII record. The CaII index is similarly defined. More accurate proxy models employ spatially resolved observations of the full solar disc, which account for the center-to-limb variation of spot and facular contrasts at least at one wavelength (e.g., Chapman, Cookson & Dobias 1996; Chapman, Cookson & Preminger 2012; Preminger, Walton & Chapman 2002). More details on proxy models can be found in reviews by Fröhlich & Lean (2004) and Domingo et al. (2009).

With time, more physics-based models have been developed (e.g., Ermolli, Criscuoli & Giorgi 2011; Fligge, Solanki & Unruh 2000; Fontenla et al. 2011; Krivova et al. 2003; Shapiro et al. 2010; Wenzler et al. 2006). They still use different (spatially resolved or disc-integrated) observations or proxies of solar magnetic activity to describe the evolution of the surface coverage by different types of solar features (such as spots or faculae), also called components of the solar atmosphere. But the brightness of each component is calculated using radiative transfer codes from semiempirical models of different features in the solar atmosphere (see, e.g., Fontenla et al. 1999, 2009; Kurucz 1993; Shapiro et al. 2010; Unruh, Solanki & Fligge 1999). Brightnesses of the

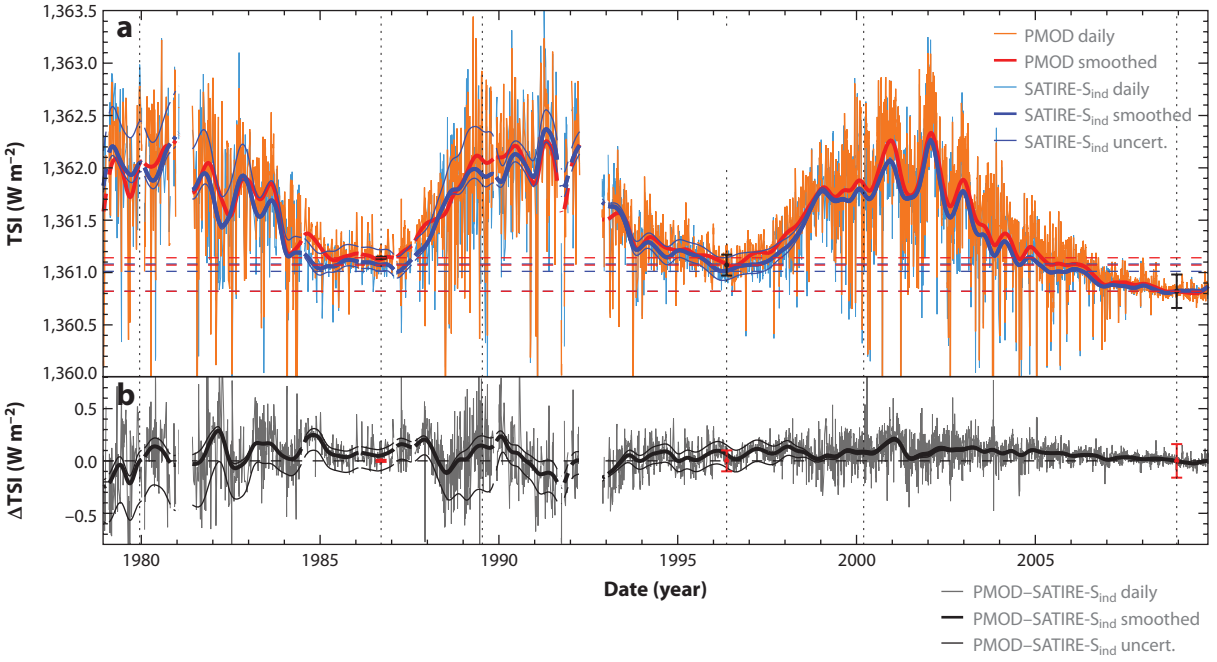

Figure 6

(*a*) Total solar irradiance (TSI) between 1978 and 2009 as given by the PMOD composite record of measurements (*light red curve* for daily and *thick red* for smoothed data) and as computed with the SATIRE-S model (*light blue* and *thick blue* for daily and smoothed data, respectively). Both data sets are normalized to SORCE/TIM data in December 2008. The thin blue lines indicate the uncertainty range of the model. Dashed horizontal lines mark TSI levels at cycle minima. Dotted vertical lines indicate cycle maxima and minima. Black error bars are the PMOD TSI errors from Fröhlich (2009). (*b*) The difference between PMOD and SATIRE-S TSI (*gray*, daily; *black*, smoothed). The PMOD TSI error bars are shown in red. Credit: Ball et al. (2012), reproduced with permission ©ESO. Abbreviations: PMOD, Physikalisch-Meteorologisches Observatorium Davos; SATIRE-S, Spectral and Total Irradiance Reconstructions for the Satellite era; SORCE, *Solar Radiation and Climate Experiment*; TIM, Total Irradiance Monitor.

photospheric components computed in this way depend on the wavelength and the heliocentric position. This brings two advantages: (*a*) it allows calculation of the spectral irradiance, which is less straightforward with proxy models, and (*b*) it takes into account the center-to-limb variation of the contrasts of different magnetic components, which provides more accurate reconstructions of solar irradiance. A successful example is the SATIRE-S (Spectral and Total Irradiance Reconstructions for the Satellite era) model employing daily solar magnetograms and continuum images (Ball et al. 2012, Krivova et al. 2003, Wenzler et al. 2006).

Spectral and Total Irradiance Reconstructions (SATIRE): a semiempirical model developed at Max-Planck-Institut für Sonnensystem-forschung (MPS)

In the past decade, significant progress has been made in modeling TSI (Ball et al. 2012; Chapman, Cookson & Preminger 2012; Ermolli, Berrilli & Florio 2003; Krivova et al. 2003; Lean et al. 2005; Preminger, Walton & Chapman 2002; Wenzler et al. 2006). State-of-the-art models reproduce more than 90% of the measured TSI variations over the whole period covered by observations (see **Figure 6**) and more than 95% for cycle 23 (Ball et al. 2011, 2012; Chapman, Cookson & Preminger 2012) when compared with the PMOD composite (see Section 2.1).

The models can in principle be used to distinguish between the composites. On the solar cycle and longer timescales, Wenzler, Solanki & Krivova (2009), Krivova, Solanki & Wenzler (2009), and Ball et al. (2012) found the SATIRE-S model to be in best agreement with the PMOD composite (**Figure 2**), although after the removal of long-term trends, the best agreement is

reached with the RMIB composite. Kopp & Lean (2011) obtain similar correlations between their proxy model (see below in this section) and the RMIB ($r_c = 0.92$) and PMOD ($r_c = 0.91$) composites.

Naval Research Laboratory Solar Spectral Irradiance (NRLSSI): a proxy irradiance model widely used in climate simulations

Development of climate models including chemistry and, thus, increased interest in solar UV data has stimulated advances to SSI modeling. Over the years, a number of models describing the variation of SSI have been constructed. These include the NRLSSI (Naval Research Laboratory Solar Spectral Irradiance; Lean 2000, Lean et al. 1997), SATIRE-S (Ball 2012; Krivova, Solanki & Floyd 2006; Krivova, Solanki & Unruh 2011; Krivova et al. 2009), the COSI (COde for Solar Irradiance; Shapiro et al. 2010, 2011), SRPM (Solar Radiation Physical Modeling; Fontenla et al. 1999, 2004, 2009, 2011) and OAR (Osservatorio Astronomico di Roma; Ermolli, Criscuoli & Giorgi 2011; Ermolli et al. 2013) models. Two recent models by Bolduc et al. (2012) and Thuillier et al. (2012) are limited to the UV spectral range only. An overview of SSI models has recently been completed by Ermolli et al. (2013).

These models reach different levels of complexity, make partly different assumptions (with the common main underlying assumption being that evolution of the magnetic field at and above the solar surface is the main cause of SSI variability), and show partly significant differences in their results (as discussed below). Nonetheless, they do have some important traits in common that are worth stressing [with one exception, the SRPM model by Fontenla et al. (2011), discussed later in this section].

1. All models produce a generally increasing level of SSI variability with decreasing wavelength in the UV. This is in qualitative agreement with the measurements (see **Figure 3*b***), whereas quantitative comparisons are discussed below.
2. On solar rotation timescales, the models and data agree remarkably well, at least for the more advanced models. This is illustrated by **Figure 7*a***, which shows daily normalized SORCE data (*red*, SIM; *orange*, SOLSTICE), UARS/SUSIM data (*green*), and three different models in the spectral range 220–240 nm over the period of 2003–2009.
3. On the solar cycle timescale, the UV variability displayed by all models is much lower (by factors of 2–6) than that shown by the SSI instruments on SORCE, although for the more advanced models it agrees rather well with the variations found by the SSI instruments on UARS. **Figure 7*b*** shows three-month smoothed values of solar irradiance at 220–240 nm between 1993 and 2009, calculated with the NRLSSI (*black curve*), SATIRE-S (*blue*), and COSI (*magenta*; yearly values) models and measured by UARS/SOLSTICE (*darker green*), UARS/SUSIM (*lighter green*), SORCE/SOLSTICE (*orange*), and SORCE/SIM (*red*). In this spectral range, all three models agree well with each other over the whole period of 1993–2009, as well as with the UARS data between 1993 and 2005 (SUSIM stopped operating in August 2005 and UARS/SOLSTICE in 2002). But the 220–240-nm flux measured by the SORCE instruments over the period of 2004–2008 decreased by a factor of four (SOLSTICE) to seven (SIM) more than expected from the models. The difference between the trend measured by SORCE/SOLSTICE and reconstructed by the models actually lies within the 3-σ long-term instrumental uncertainty (Unruh, Ball & Krivova 2012). The discrepancy between the models and SIM is larger, but in this spectral range SIM is considered to be less accurate than SOLSTICE.
4. The SSI variability is in phase with the solar cycle at all wavelengths (with the exception of a short stretch in the IR). This disagrees with the data from SORCE/SIM (cf., the *green curve* showing the SATIRE-S model, and the *dotted part of the blue curve* showing SIM data at antiphase with the cycle in **Figure 3**).

Although qualitatively the results of most models are similar, they also show significant quantitative differences. Most important for climate models is the discrepancy in the estimated UV

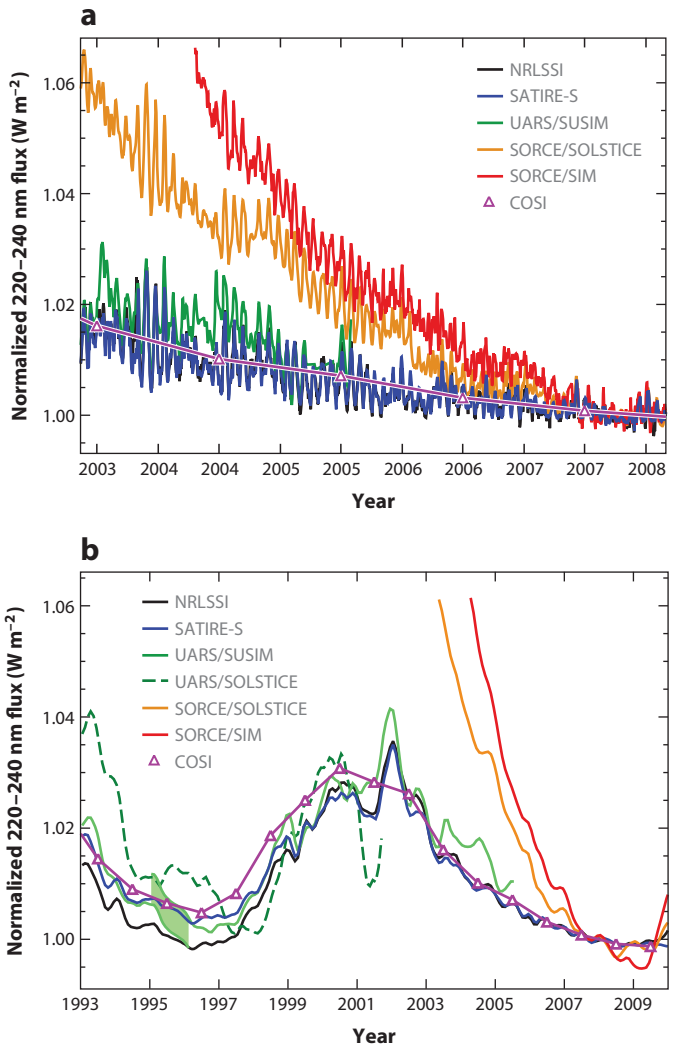

Figure 7

Normalized solar UV irradiance between 220 and 240 nm calculated with NRLSSI (*black*), SATIRE-S (*blue*), and COSI (*magenta*) models and measured with UARS/SUSIM (*darker green*), UARS/SOLSTICE (*light green*), SORCE/SOLSTICE (*orange*), and SORCE/SIM (*red*). The pale green shading marks the period when the sensitivity of the UARS/SUSIM instrument (and thus the flux) changed, so that a shift was applied to the data before that (see Krivova, Solanki & Floyd 2006 and Krivova et al. 2009 for details). Panel *a* is limited to the period when SORCE was in operation, i.e., after 2003, and shows daily values, except for the COSI model, for which only yearly averages are available. Panel *b* shows three-month smoothed values over the period of 1993–2009, for which UARS and/or SORCE data are available. Reprinted from Ermolli et al. (2013). Abbreviations: COSI, Code for Solar Irradiance; NRLSSI, Naval Research Laboratory Solar Spectral Irradiance; SATIRE-S, Spectral And Total Irradiance Reconstructions for the Satellite era; SIM, Spectral Irradiance Monitor; SOLSTICE, Solar Stellar Irradiance Comparison Experiment; SORCE, *Solar Radiation and Climate Experiment;* SUSIM, Solar Ultraviolet Spectral Irradiance Monitor; UARS, *Upper Atmosphere Research Satellite*.

variability at 250–400 nm, where models differ by up to a factor of three, e.g., between NRLSSI and COSI. On the one hand, proxy models generally tend to underestimate the variability in this range. Such models rely on SSI measurements, at least in this spectral range [e.g., NRLSSI and the models by Pagaran, Weber & Burrows (2009) or Thuillier et al. (2012)], and extrapolate observed rotational variability to longer timescales.

On the other hand, model atmospheres of the solar features employed in semiempirical SSI models (e.g., in SATIRE-S, COSI, SRPM, and OAR) have not yet been tested observationally at all wavelengths (due to the lack of appropriate observations) and have some freedom as well, although they cannot be tuned arbitrarily. An example is given by the SRPM model (Fontenla et al. 2011), in which the atmospheric models were tuned to allow better agreement with the SORCE SSI data. Thus it is the only model that qualitatively reproduces SORCE/SIM SSI behavior, in particular, the reversed variability in the visible. This is, however, achieved at the expense of TSI: The modeled TSI does not reproduce the solar cycle change, which is measured much more reliably than the SSI. Interestingly, the OAR model uses essentially the same input as SRPM, with the earlier untuned versions of the same atmospheric models (Fontenla et al. 2009), and is able to reproduce the TSI changes but not the SORCE SSI variability (Ermolli et al. 2013). The difference in the predicted variability at 250–400 nm between semiempirical models (excluding SRPM, i.e., considering only models that reproduce the TSI variability) is still almost a factor of two, with COSI showing the strongest variability and OAR the weakest. A more detailed comparison of the models has been presented by Ermolli et al. (2013).

Maunder minimum: the most famous example of a grand minimum that occurred in the seventeenth century

grand minimum (maximum): multidecade period of low (high) solar activity

Little Ice Age (LIA): a period of cooling in the Northern Hemisphere, the coldest part occurring around the seventeenth century

3. LONGER TERM SOLAR VARIABILITY: SECULAR CHANGE OF IRRADIANCE

3.1. Grand Maxima and Minima

The longest running record of solar activity, available since 1610, is the sunspot number (observations started only one year after the invention of the telescope in 1609). It is a simple measure of the Sun's activity, but nonetheless rather robust, especially when only sunspot groups are counted [as is the case for the group sunspot number introduced by Hoyt & Schatten (1998)]. Robustness is a necessary condition because data from different sources need to be combined in building up any long-running solar activity record. The most striking feature of this record, plotted in **Figure 8**, is the solar activity cycle. Each cycle lasts between 8 and 14 years, with an average length of approximately 11.2 years. Cycle amplitudes vary even more strongly, with the weakest known cycle (starting around 1700) being less than 10% in strength of the strongest cycle, cycle 19, although in the minima between the cycles the sunspot number reaches nearly zero (there are some differences between minima following very strong cycles and those following weaker cycles). The solar cycle has been reviewed in detail by Hathaway (2010).

Almost as striking as the presence of the cycles is their absence, along with the near absence of sunspots themselves, between roughly 1640 and 1700 (Eddy 1976, Soon & Yaskell 2003). This Maunder minimum is a prime example of a grand minimum of solar activity, which in this case overlapped with a particularly cold part of the Little Ice Age (LIA). Grand minima of solar activity have been reviewed by Usoskin, Solanki & Kovaltsov (2012).

The only direct records of solar activity measurements that reach further back in time are scattered naked-eye sightings of sunspots, mainly in China (Yau & Stephenson 1988). These are too scarce to allow a reliable reconstruction of solar activity. An alternative is provided by cosmogenic isotopes, such as ^{14}C and ^{10}Be stored in terrestrial archives. These isotopes are produced in Earth's atmosphere by nuclear reactions (neutron capture, spallation) between energetic cosmic

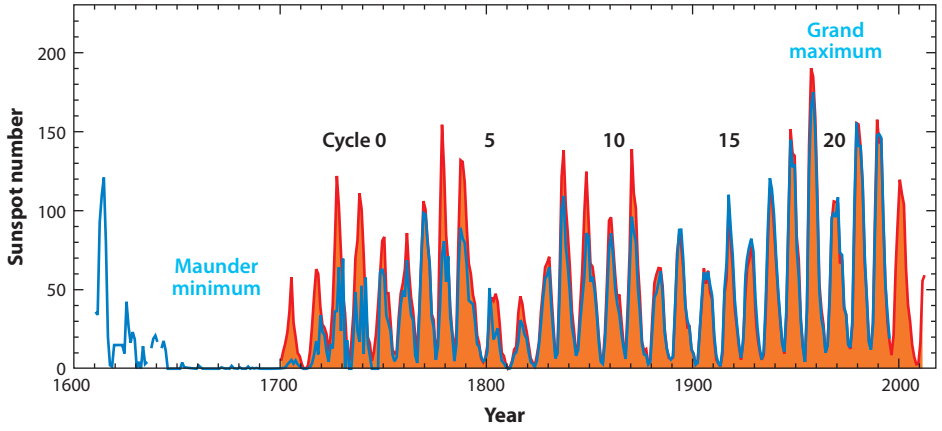

Figure 8

Telescopic, yearly averaged, sunspot number records: Zurich (*orange*) and group sunspot number (*blue*; Hoyt & Schatten 1998, Sol. Influ. Data Anal. Cent. 2011, Vaquero et al. 2011). The Zurich (or Wolf) number was introduced by Rudolf Wolf in the 1840s, the group number by Hoyt & Schatten (1998). The group sunspot number has been proposed to better represent actual level of activity before 1880, but is not yet officially available for cycles 23 and 24.

rays and constituents of Earth's atmosphere (mainly N, but also O and Ar in the case of ^{10}Be). After production, the two main cosmogenic isotopes take different paths. ^{14}C becomes part of the global carbon cycle until it ends up in one of the sinks, e.g., the ocean or in plant material. Of interest are those atoms that end up in the trunks of datable trees. After circulating in the atmosphere for a few years, if it was formed in the stratosphere, ^{10}Be precipitates and can be recovered (and dated) if it is deposited on striated ice sheets, such as those of Greenland or Antarctica.

Because both isotopes are radioactive (half-lives of 5,730 years for ^{14}C and 1.36×10^6 years for ^{10}Be) and have no terrestrial sources, their concentration in a layer (or year-ring) of their natural archives is a measure of the production rate of these isotopes at the time of deposition (after relevant corrections). This, in turn, depends on the flux of cosmic rays reaching Earth's atmosphere, which is mainly determined by the strength (and, at least for ^{10}Be, the geometry) of Earth's magnetic field, and on the level of solar activity. Hence, if the geomagnetic field is known from a previous reconstruction (e.g., Knudsen et al. 2008, Korte & Constable 2005), then the level of solar activity, primarily modulation potential, which depends mainly on the Sun's open magnetic flux, can be determined using a simple model.

A further important requirement for ^{14}C is that ocean circulation remains roughly unchanged (which can be shown for the Holocene; Stuiver 1991). The ^{10}Be, in turn, may be sensitive to variations in local climate (e.g., Field et al. 2006).

The connection of the open magnetic flux with the quantities needed to estimate solar irradiance variations, sunspot and facular areas, or alternatively sunspot number and total magnetic flux, can then be established via another simple model introduced by Solanki, Schüssler & Fligge (2000, 2002; cf. Vieira & Solanki 2010). The main ingredient of this model is that solar cycles overlap due to two mechanisms: (*a*) magnetic flux belonging to the new cycle starts to emerge while flux belonging to the old cycle is still emerging and (*b*) magnetic flux organized on large scales (i.e., mainly the open flux) decays very slowly, over a timescale of years, and hence is still present when the next cycle is well underway.

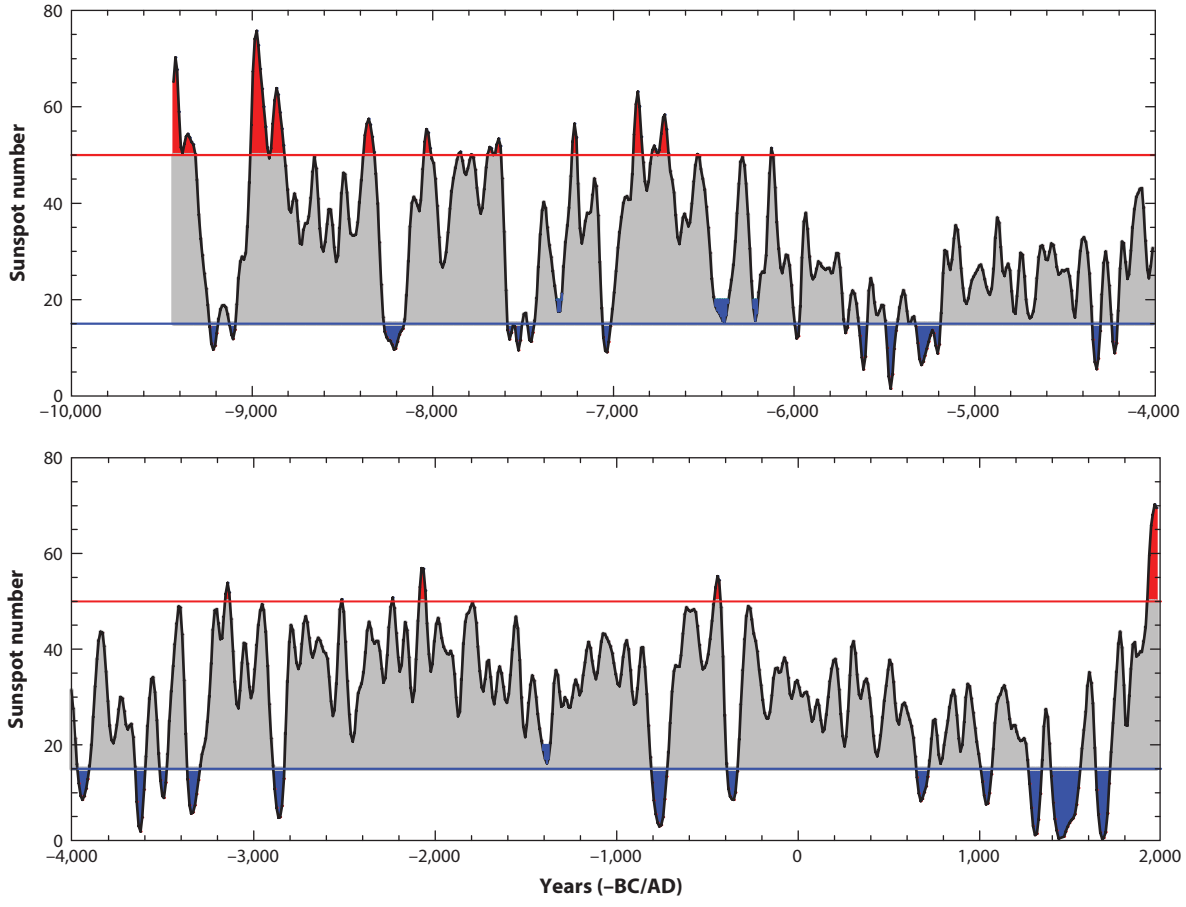

Figure 9

Sunspot numbers for the last 11,400 years reconstructed from ^{14}C. The original 10-year sampled data have been smoothed with a 1-2-2-2-1 filter prior to plotting. Red and blue areas denote grand maxima and minima, respectively. Credit: Usoskin, Solanki & Kovaltsov (2007), reproduced with permission ©ESO.

Usoskin et al. (2004) have shown that by putting together the various models solar activity can be reconstructed reliably, at least from ^{14}C. This was put to use by Usoskin et al. (2003b), who reconstructed sunspot numbers for the last 1,000 years, and by Solanki et al. (2004), who did so for the last 11,400 years, i.e., basically the full Holocene. Reconstructions of solar activity based on ^{10}Be followed later (Steinhilber, Abreu & Beer 2008; Steinhilber, Beer & Fröhlich 2009). Although the reconstructions based on the two isotopes (and to some extent those based on different geomagnetic field reconstructions) differ from each other in detail, they show a similar statistical behavior (Steinhilber et al. 2012, Usoskin et al. 2009). Such model-based reconstructions supersede earlier work by, e.g., Stuiver & Braziunas (1989) with ^{14}C.

The reconstructed (smoothed) sunspot number is plotted in **Figure 9**. Clearly, there have been a number of periods of very low activity similar to the Maunder minimum. Periods having a sunspot number below 15 for at least 20 years are defined as grand minima, whereas a sunspot number above 50 for the same length of time gives a grand maximum. Other definitions are also possible (see, e.g., Abreu et al. 2008).

Grand minima and maxima are almost randomly distributed, although grand minima tend to come in clusters separated by roughly 2,000–3,000 years. Unlike the grand maxima, whose duration follows an exponential distribution, the grand minima come in two varieties, a short (30–90 year) type, with the Maunder minimum being a classic example, and a long (>110 year) type, such as the Spörer minimum (1390–1550).

The last grand maximum of solar activity has only just ended. As Usoskin et al. (2003a) and Solanki et al. (2004) showed, the Sun entered a grand maximum period in the middle of the twentieth century, characterized by strong sunspot cycles, short, comparatively active minima, a high value of the Sun's open magnetic flux, and plentiful other indicators of vigorous solar activity. This grand maximum has now ended as had been expected by Solanki et al. (2004) and later by Abreu et al. (2008). This is indicated by the long and very quiet activity minimum between cycles 23 and 24 (2005–2010) and the weak currently running cycle.

Making predictions about how the activity will develop in future is not at present possible beyond the maximum of the current cycle. Thus only statistical estimates of future solar activity can be made based on comparisons with the reconstructed long-term activity record (Abreu et al. 2008, Lockwood 2009, Solanki & Krivova 2011, Solanki et al. 2004). In particular, it is unlikely that the Sun will slip into a grand minimum (less than 8% likelihood within the next 30 years; Lockwood 2009), and it is equally likely that the next grand extremum will be a grand maximum as a grand minimum.

3.2. By How Much Did the Sun Vary Between the Maunder Minimum and Now?

The sunspot number is a good representative of the solar magnetic activity cycle. Hence historical records of sunspot numbers since 1610 (Hoyt & Schatten 1998) and sunspot areas since 1874 (e.g., Balmaceda et al. 2009 and references therein) allow decent reconstructions of the cyclic component of solar irradiance changes over the past four centuries. All such reconstructions show that in the past few decades the Sun was unusually active (see previous section), so that the cycle-average TSI was also roughly 0.6 W m^{-2} higher than during the Maunder minimum (Solanki & Fligge 2000) even in the absence of any secular change.

Reconstructions of the heliospheric magnetic field from the geomagnetic aa-index and observations of the interplanetary magnetic field imply that the Sun's open magnetic field increased by nearly a factor of two since the end of the nineteenth century (Lockwood, Stamper & Wild 1999; Lockwood, Rouillard & Finch 2009) before dropping again to the nineteenth century values in the past few years. The total photospheric magnetic flux, which is more directly related to solar irradiance, has been regularly measured for only about four decades (e.g., Arge et al. 2002; Wang, Sheeley & Rouillard 2006), so that longer term changes cannot yet be reliably assessed. Harvey (1993, 1994) noticed, however, that small ephemeral active regions keep bringing copious amounts of magnetic flux to the solar surface during activity minima, when active regions are rare or absent. The magnetic flux provided by the ephemeral regions, and concentrated in the network in the quiet Sun, varies little over the activity cycle as ephemeral regions belonging to two different solar cycles emerge in parallel for multiple years (Hagenaar, Schrijver & Title 2003; Harvey 1992, 1993, 1994). The overlap between the cycles provides a physical explanation for the secular change in the photospheric magnetic field and irradiance (Solanki, Schüssler & Fligge 2000, 2002).

The magnitude of the secular change remains, however, heavily debated. This is because the sunspot numbers or areas widely employed in the reconstructions on timescales longer than a few decades are related only indirectly to the amount of flux emerging in small ephemeral regions feeding the magnetic network.

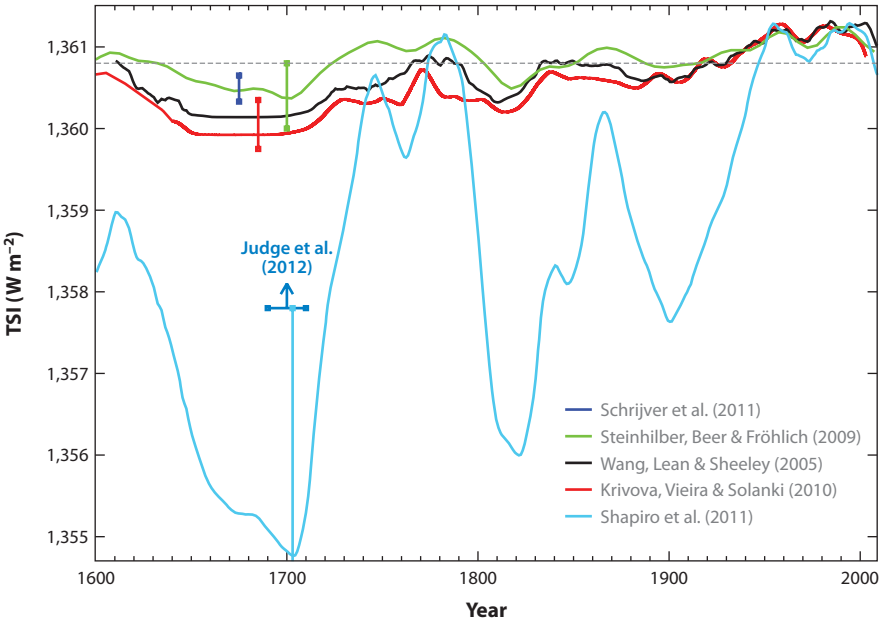

Figure 10

Various total solar irradiance (TSI) reconstructions since 1600 identified in the plot. The dark blue vertical bar shows the possible range of the TSI change following Schrijver et al. (2011; no reconstruction available). Other vertical bars denote uncertainties of the models, plotted in same colors. Note that the uncertainty in the Shapiro et al. (2011) model, ± 3 W m^{-2}, extends downward outside the plot, and the blue horizontal bar and arrow mark the reduced value of this model as argued by Judge et al. (2012). The black dotted line shows the TSI value representing solar minimum conditions following *Solar Radiation and Climate Experiment* (SORCE)/Total Irradiance Monitor (TIM) measurements.

The first estimates of the change in TSI since the Maunder minimum, mainly derived from solar-stellar comparisons, ranged from 2 to 16 W m^{-2} (Lean, Skumanich & White 1992; Mendoza 1997; Zhang et al. 1994). They were indirect and based on a number of assumptions that were later found to be spurious (e.g., Hall et al. 2009, Hall & Lockwood 2004, Wright 2004). Judge et al. (2012) argue that current stellar data do not yet allow an assessment of the secular change in the solar brightness, and longer stellar observations are required.

Various empirical reconstructions produced in the 2000s give values between 1.5 and 2.1 W m^{-2} (e.g., Foster 2004, Lockwood 2005, Mordvinov et al. 2004). Lockwood & Stamper (1999) were the first to apply a linear relationship between the open magnetic flux and the TSI derived from the data obtained over the satellite period. Later, such a linear relationship was also employed by Steinhilber, Beer & Fröhlich (2009) to reconstruct TSI from the ^{10}Be data. This reconstruction covers the whole Holocene and is discussed in Section 3.3, where we also consider the validity of the linear relationship. Their reconstruction for the period after 1610 is shown in **Figure 10** together with a number of other recent reconstructions. The derived TSI increase since 1710 is 0.9 ± 0.4 W m^{-2}. Note that due to the uncertainties in the TSI levels during the last three activity minima (see Sections 2.1 and 2.3) used to construct the linear relationship, the uncertainty of this model is also relatively high.

Models that are more physics-based were employed by Wang, Lean & Sheeley (2005), Krivova, Balmaceda & Solanki (2007) and Krivova, Vieira & Solanki (2010). Wang, Lean & Sheeley (2005)

used a surface flux transport simulation of the evolution of the solar magnetic flux combined with the NRLSSI irradiance model (see Section 2.3). Krivova, Balmaceda & Solanki (2007) and Krivova, Vieira & Solanki (2010) have reconstructed the evolution of the solar magnetic flux from the sunspot number with the 1D model of Solanki, Schüssler & Fligge (2000, 2002) and Vieira & Solanki (2010) and then used the SATIRE model (Section 2.3) to reconstruct the irradiance. This combination is called SATIRE-T (for telescopic era). They found that the cycle-averaged TSI was about $1.3^{+0.2}_{-0.4}$ W m^{-2} higher in the recent period compared with the end of the seventeenth century, in agreement with the assessments by Foster (2004), Lockwood (2005), and Wang, Lean & Sheeley (2005). Both SATIRE-T and NRLSSI models are shown in **Figure 10**.

Most of the models are tested against the directly measured TSI and reproduce it fairly well. However, as the secular change over the satellite period is quite weak, if any, and is not free of uncertainties, as indicated by the difference between the three composites (see Sections 2.1 and 2.3, as well as **Figures 2** and **6**), these data are not well suited to constrain the rise in TSI since the Maunder minimum. For this reason, the SATIRE model is also tested against other available data sets. Thus the modeled solar total and open magnetic flux are successfully compared to the observations of the total magnetic flux over the past four decades and the empirical reconstruction of the heliospheric magnetic flux from the aa-index over the past century, respectively. Also, the activity of the ^{44}Ti isotope (Usoskin et al. 2006) calculated from the SATIRE-T open flux agrees well with ^{44}Ti activity measured in stony meteorites (Vieira et al. 2011). Finally, the reconstructed irradiance in Lyα agrees with the composite of measurements and proxy models by Woods et al. (2000) going back to 1947 (Krivova, Vieira & Solanki 2010).

Recently, Schrijver et al. (2011) argued that the last minimum in 2008, which was deeper and longer compared to the eight preceding minima, might be considered a good representative of a grand minimum. This would mean a secular decrease of only about 0.15–0.5 W m^{-2} (estimated as the difference between TSI in the PMOD composite during the minima preceding cycles 22 and 24 in 1986 and 2008, respectively; Fröhlich 2009). If the cycle averaged 0.6 W m^{-2} TSI change due to the cyclic component (Solanki & Fligge 2000) is added to this, the total increase would be about 0.75–1.1 W m^{-2}. (Note that most sources list the sum of the modeled cyclic and secular components of the irradiance change since the Maunder minimum.)

A very different estimate was published by Shapiro et al. (2011), who assumed that during the Maunder minimum the entire solar surface was as dark as is currently observed only in the dimmest parts of supergranule cells (in their interiors). To describe this quiet state, Shapiro et al. (2011) employed the semiempirical model atmosphere A by Fontenla et al. (1999; see Section 2.3), which gave a rather large TSI increase of 6 ± 3 W m^{-2} since the Maunder minimum. This reconstruction is also shown in **Figure 10**. Judge et al. (2012) have recently argued, based on the analysis of submillimeter data, that by adopting model A Shapiro et al. (2011) overestimated quiet-Sun irradiance variation by about a factor of two, so the modeled increase in TSI since the Maunder minimum is overestimated by the same factor.

Foukal & Milano (2001) argued on the basis of uncalibrated historic CaII photographic plates from the Mt. Wilson Observatory that the area coverage by the network did not change over the twentieth century, which would imply no or very weak secular change in the irradiance. A number of observatories around the globe carried out full-disc solar observations in the CaII K line since the beginning of the twentieth century, and some of these have recently been digitized. Ermolli et al. (2009) have shown, however, that such historical images suffer from numerous problems and artifacts. Moreover, calibration wedges are missing on most of the images, making proper intensity calibration a real challenge. Without properly addressing these issues, results based on historic images must be treated with caution. In summary, present-day estimates of the TSI change since the end of the Maunder minimum range from 0.8 W m^{-2} to about 3 W m^{-2}, i.e., over nearly a

factor of four. In addition, the time dependence also is different in the various reconstructions and is rather uncertain.

3.3. Variation over the Holocene

In their 2004 review, Fröhlich & Lean concluded that "Uncertainties in understanding the physical relationships between direct magnetic modulation of solar radiative output and heliospheric modulation of cosmogenic proxies preclude definitive historical irradiance estimates, as yet." Since then, this topic has progressed rapidly, and we now have several reconstructions of TSI over the Holocene. These build upon the reconstructions of solar activity indices (modulation potential, open flux, total flux, etc.) described in Section 3.1, although only cycle-averaged values of irradiance can be reconstructed prior to 1610.

Because the modulation potential, Φ, is the primary quantity obtained from the production rates of cosmogenic isotopes (Section 3.1), it serves as an input to all irradiance reconstructions on millennial timescales. But the methods are different. Thus the Shapiro et al. (2011) scale irradiance changes linearly with the 22-year averaged Φ calculated by Steinhilber, Beer & Fröhlich (2009) from ^{10}Be data. As discussed in Section 3.2, the magnitude of the secular change is derived in this model from a comparison of the current Sun at activity minimum conditions with the semiempirical model atmosphere describing the darkest parts of the intergranule cells, and the model shows a significantly stronger variability compared to other models (**Figure 10**).

In fact, the relationship between irradiance and Φ is not straightforward (Steinhilber, Beer & Fröhlich 2009; Usoskin et al. 2002; Vieira et al. 2011). Therefore Steinhilber, Beer & Fröhlich (2009) and Vieira et al. (2011) first employ physical models to calculate the solar open magnetic flux from Φ (see also Solanki et al. 2004, Usoskin et al. 2002, 2003a). TSI is then reconstructed in the model by Steinhilber, Beer & Fröhlich (2009) through a linear empirical relationship between the directly measured open magnetic flux and TSI during the three recent activity minima. Vieira et al. (2011), in contrast, apply a physical model (Vieira & Solanki 2010) to compute the sunspot number and the total magnetic flux from the reconstructed open flux and to show that irradiance is modulated by the magnetic flux from two consecutive cycles (which is not so surprising; see Section 3.2). Thus irradiance can be represented by a linear combination of the jth and jth+1 decadal values of the open flux. This implies that although employment of a linear relationship between TSI and the open flux is not justified physically, it might work reasonably on timescales longer than several cycles.

The reconstruction of TSI over the Holocene by Vieira et al. (2011) using the SATIRE-M (for Millennia) model is plotted in **Figure 11**. For comparison, the reconstruction from the telescopic sunspot record (SATIRE-T; see Section 3.2) is also shown. In general, the various TSI reconstructions over the Holocene display similar longer term dependences (Steinhilber et al. 2012), with the main difference being the amplitude of the variations (see Section 3.2). Thus the reconstruction by Steinhilber, Beer & Fröhlich (2009) shows a somewhat weaker variability, as can be judged from **Figure 10** over the telescopic era.

4. INFLUENCE OF SOLAR VARIABILITY ON CLIMATE

4.1. Evidence of Solar Influence on Climate on Different Timescales

The role of the Sun in producing daily and seasonal fluctuations in temperature, and their distribution over Earth, seems so obvious that it might be thought self-evident that variations in solar activity influence weather and climate. This idea has, however, been controversial over many

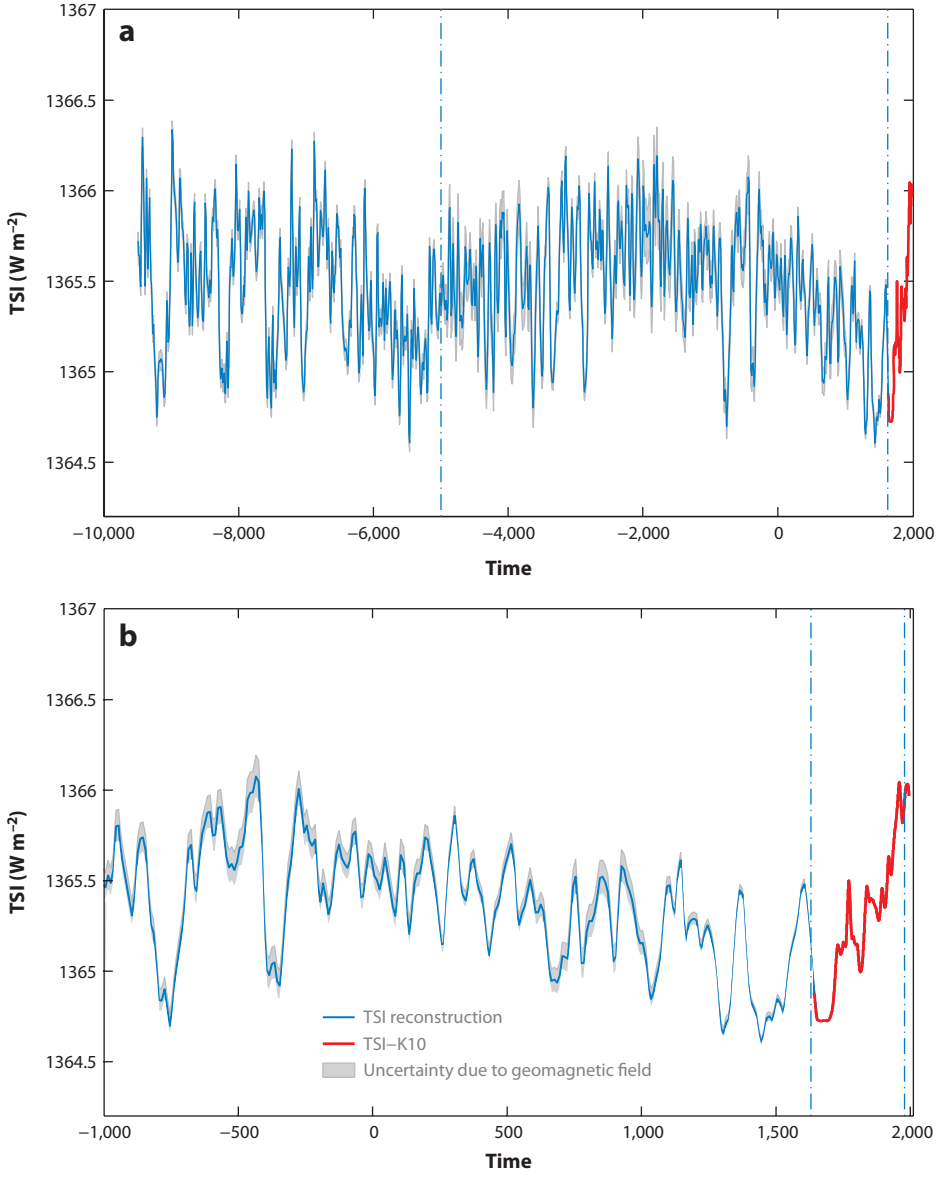

Figure 11

(*a*) Total solar irradiance (TSI) reconstruction since 9500 BC using the SATIRE-M (Spectral and Total Irradiance Reconstructions for Millennia; *blue*) and SATIRE-T (for telescopic era; *red*) models. (*b*) Enlargement of panel *a* for the last 3,000 years. The gray shading marks the uncertainty due to different reconstructions of the geomagnetic field. Credit: Vieira et al. (2011), reproduced with permission ©ESO.

centuries. The reasons for this skepticism center around three areas: first, the insubstantial nature of much of the meteorological "evidence"; second, a lack of adequate data on variations in solar energy reaching Earth; and third, related to the second, a lack of any plausible explanation for how the proposed solar influence might take place. Since the advent of Earth-orbiting satellites, however, we have substantial evidence for variations in solar output, as discussed in Section 2, and

this, together with meteorological records of increasingly high quality and coverage, are facilitating advances in understanding solar signals in climate. Below we present some of the evidence for a solar influence at Earth's surface, as well as in the middle and lower atmospheres, and go on to discuss the processes that might produce these signals.

4.1.1. Surface. Much work concerned with solar influences on climate has focused on the detection of solar signals in surface temperature. It has frequently been remarked that the Maunder minimum in sunspot numbers in the second half of the seventeenth century coincided with the LIA during which most of the proxy records (indicators of temperature including cosmogenic isotopes in tree rings, ice cores and corals as well as documentary evidence) show cooler temperatures. Care needs to be taken in such interpretation as factors other than the Sun may also have contributed. The higher levels of volcanism prevalent during the seventeenth century, for example, would also have introduced a cooling tendency due to a veil of particles injected into the stratosphere reflecting the Sun's radiation back to space, and this is discussed further in Section 4.2.1 below.

Evidence from a variety of sources, however, does suggest that during the LIA the climate of the Northern Hemisphere was frequently characterized by cooler-than-average temperatures in eastern North America and western Europe, and warmer-than-average temperatures in Greenland and central Asia. This pattern is typical of a negative phase of a natural variation in climate referred to as the North Atlantic Oscillation (NAO). Indeed, temperature maps constructed from a wide selection of proxy temperature data typically give the spatial pattern of temperature difference between the Medieval Climate Anomaly (MCA, c. 950–1250) and the LIA, showing a pattern similar to a positive NAO.

Across the Holocene (the period of about 11,700 years since the last Ice Age), isotope records from lake and marine sediments, glaciers, and stalagmites provide evidence that solar grand maxima/minima affect climate, although these studies all rely on the reliability of the dating, which is complex and not always precise. The records show strong regional variations typically including an NAO-like signal, as outlined above, and also a pattern similar to a La Niña event [this is the opposite phase of the ENSO (El Niño Southern Oscillation) cycle to El Niño and is associated with cold temperatures in the eastern Pacific Ocean] and to greater monsoon precipitation in southern Oman [see, e.g., the review by Gray et al. (2012)].

One approach, using a multiple linear regression analysis to separate different factors contributing to global mean surface temperature over the past century, is illustrated in **Figure 12**. This suggests that the Sun may have introduced an overall global warming (disregarding the 11-year cycle modulation) of approximately 0.07 K before about 1960, but that it has had little effect since. Over the century, the temperature has increased by about 1 K, so the fractional contribution to global warming that can be ascribed to the Sun over the last century is 7%. This result does, however, depend fundamentally on the assumed temporal variation of the solar forcing and, as discussed in Section 3.2, there is some uncertainty in this. The index of solar variability used as the regression index in **Figure 12** was that of Wang, Lean & Sheeley (2005), which has a small long-term trend. The effect on radiative forcing (RF) of using different TSI records is further discussed in Section 4.2.1.

Crucially, however, it is not possible to reproduce the global warming of recent decades using a solar index alone. This conclusion is confirmed by studies using more sophisticated nonlinear statistical techniques.

On the timescale of the 11-year solar cycle, analyses of surface temperature and pressure show regional variations in the solar signal consistent with those found over longer periods. **Figure 13**, for example, presents the solar cycle signal in the North Atlantic region derived from 44 winters of surface temperature and pressure data (from the ERA-40 Reanalysis data set, which optimally

North Atlantic Oscillation (NAO): a pattern of climate fluctuations that controls the strength and direction of westerly winds across the North Atlantic

Medieval Climate Anomaly (MCA): a period (c. 950–1250) of warm climate in the North Atlantic region (also Medieval Warm Period or Medieval Climate Optimum)

radiative forcing (RF): the (hypothetical) instantaneous change in net radiation balance produced at the top of the atmosphere upon introduction of a perturbing factor

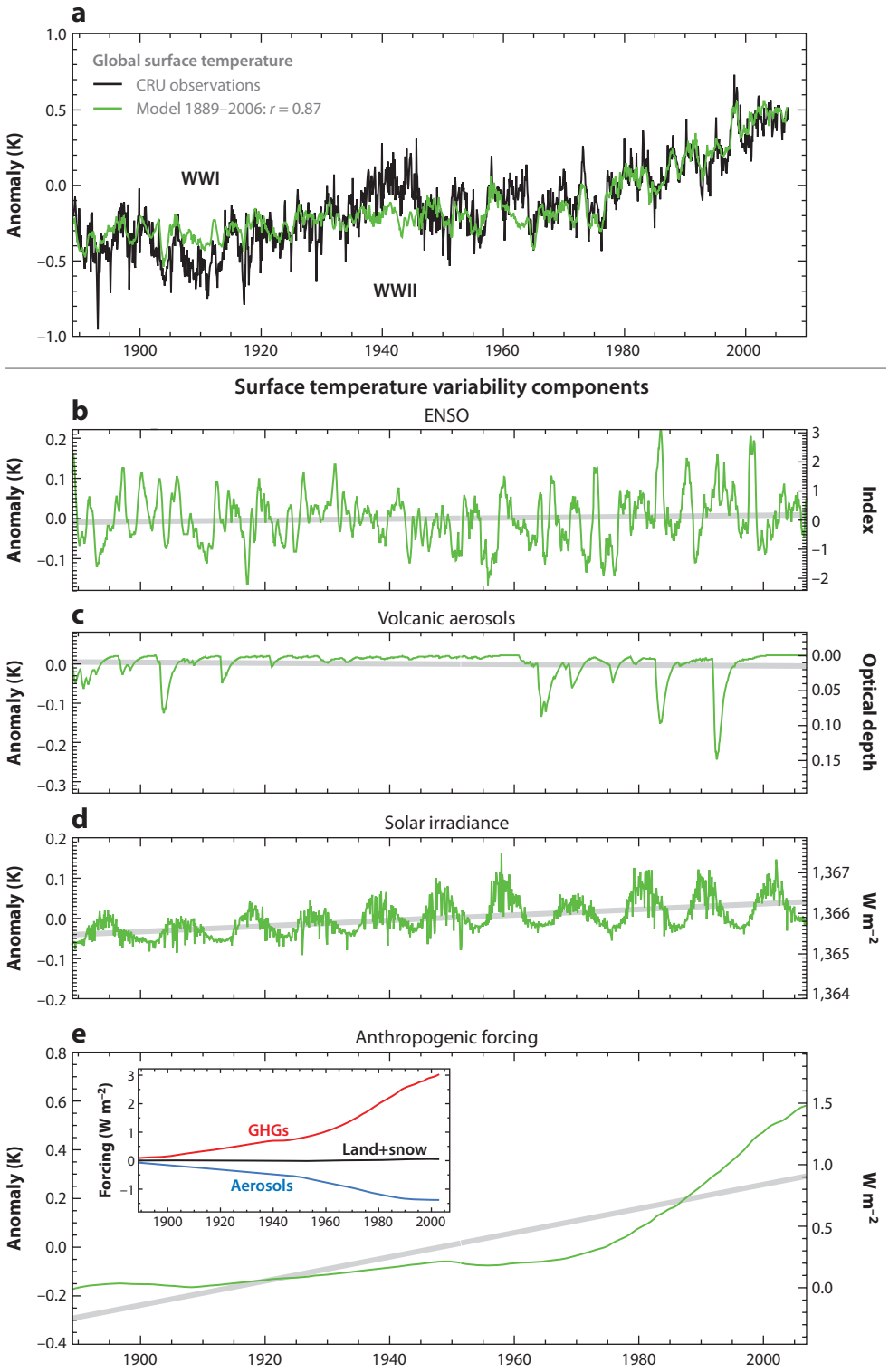

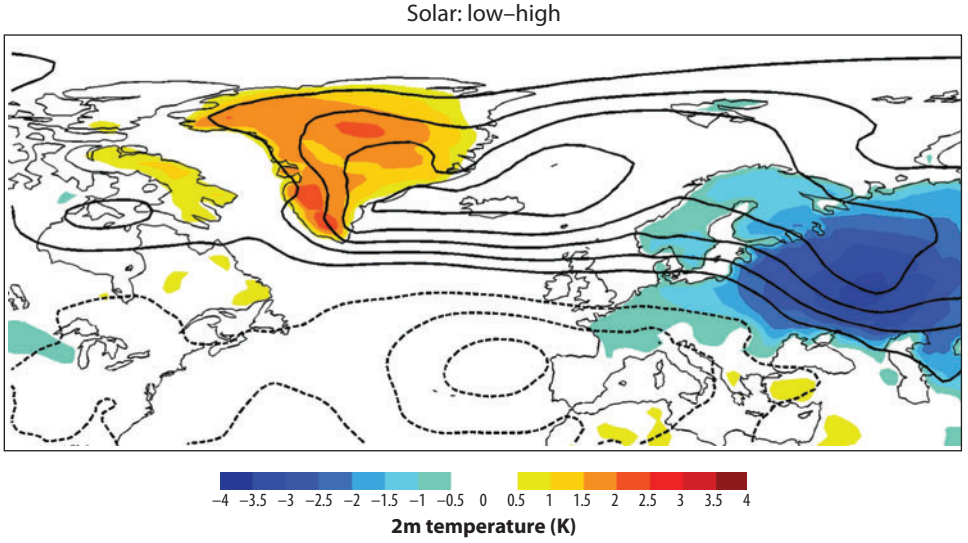

Figure 13

Difference in winter mean sea-level pressure (contours, spaced at 1 hPa with negative curves depicted as dashed curves) and near surface land temperature (colors) between periods of low and high solar activity during the period from 1957–1958 to 2000–2001. Reprinted from Woollings et al. (2010).

combines observational and model data; see Uppala et al. 2005). The result is presented for periods of low, relative to high, solar activity and resembles a negative NAO pattern. This indicates that atmospheric "blocking events," during which the jet stream is diverted in a quasi-stationary pattern associated with cold winters in Western Europe, occur more frequently when the Sun is less active.

In the North Pacific Ocean, Christoforou & Hameed (1997) found that the Aleutian Low pressure region shifts westward when the Sun is more active and the Hawaiian High northward. Solar signals in the North Pacific mean sea-level pressure have also been identified, using different techniques, by van Loon, Meehl & Shea (2007) and Roy & Haigh (2010), implying shifts in trade winds and storm tracks.

In the eastern tropical Pacific a solar cycle has been found by Meehl et al. (2008) in sea surface temperatures (SSTs), which is expressed as a cool (La Niña–like) anomaly at sunspot maximum, followed a year or two later by a warm anomaly, although with data on only 14 solar peaks available the robustness of this signal has been questioned by Roy & Haigh (2012). Analyses of tropical circulations are not conclusive, but a picture is emerging of a slight expansion of the Hadley cells (within which air rises in the tropics and sinks in the subtropics) (e.g., Brönnimann et al. 2007), a strengthening of the Walker circulation (an east-west circulation with air rising over Indonesia and sinking over the eastern Pacific), and strengthening of the South (Kodera 2004) and East (Yu et al. 2012) Asian monsoons when the Sun is more active.

←

Figure 12

(*a*) The global mean surface temperature record compiled from measurements (*black*) and its reconstruction from a multiple linear regression model (*green*). (*b–e*) The contributions associated with the four regression components. Reprinted from Lean & Rind (2008). Abbreviations: CRU, Climatic Research Unit (of the University of East Anglia); ENSO, El Niño Southern Oscillation; GHGs, greenhouse gases; WW, World War.

Such changes in circulation are associated with changes in cloudiness, and in the location and strength of regions of precipitation. A solar signal in cloudiness, however, remains difficult to establish, mainly due to the very high innate variability in clouds and also to some uncertainty in the definition of cloud types that might be affected.

4.1.2. Atmosphere. Pioneering work in Berlin used data from meteorological balloons to show correlations between stratospheric temperature and the solar 10.7-cm radio flux over an increasing number of solar cycles (see the summary by Labitzke 2001). The largest correlations were found in the mid-latitude lower stratosphere, implying temperature differences in that region of up to 1 K between minimum and maximum of the 11-year solar cycle. This response was very intriguing as it was much larger than would be expected based on understanding of variations in irradiance. Another interesting result was the large warming found in the lower stratosphere at the winter pole.

Subsequent attempts to isolate the solar effect throughout the atmosphere from other influencing factors have been carried out using multiple linear regression analysis (Haigh 2003, Frame & Gray 2010). In the middle atmosphere, the tropics show the greatest warming, of over 1.5 K in the upper stratosphere near 1 hPa, a minimum response around 5–30 hPa, and lobes of warming in the subtropical lower stratosphere. In the troposphere, maximum warming does not appear in the tropics but in mid-latitudes, with vertical bands of temperature increase around 0.4 K.

A similar analysis of zonal mean zonal (i.e., west-to-east) winds for the Northern Hemisphere winter shows, when the Sun is more active, that there is a strong positive zonal wind response in the winter hemisphere subtropical lower mesosphere and upper stratosphere. The zonal wind anomaly is observed to propagate downward with time over the course of the winter (Kodera & Kuroda 2002). In the troposphere, the wind anomalies indicate that the mid-latitude jets are weaker and positioned further poleward when the Sun is more active (Haigh, Blackburn & Day 2005). This has implications for the positions of the storm tracks and provides evidence for a solar signal in mid-latitude climate.

It is well established that stratospheric ozone responds to solar activity. The vertically integrated ozone column varies by 1–3% in phase with the 11-year solar cycle, with the largest signal in the subtropics. The vertical distribution of the solar signal in ozone is more difficult to establish because of the short length of individual observational records and problems of intercalibration of the various instruments, but in the tropics solar cycle variations appear to peak in the upper and lower stratosphere with a smaller response between.

4.2. Physical Processes

A range of physical and chemical processes, summarized in **Figure 14**, are involved in producing the observed solar signals in climate, with some being better characterized than others. About one half of the TSI entering the top of the atmosphere is transmitted to, and warms, Earth's surface so that variations in TSI have the potential to influence climate through what have become known as bottom-up mechanisms. Solar UV radiation, however, is largely absorbed by the middle atmosphere meaning that variations in UV have the potential to produce a top-down effect. In either case, the response of the atmosphere and oceans involves complex feedbacks through changes in winds and circulations so that the directive radiative effects provide only the initiating step. It is most likely that both routes for the solar influence play some role, further increasing the overall complexity.

Also indicated in **Figure 14** are processes introduced through the effects of energetic particles. GCRs, the incidence of which is modulated by solar activity, ionize the atmosphere, influencing Earth's magnetic field and possibly affecting cloud condensation. Solar energetic particles, emitted

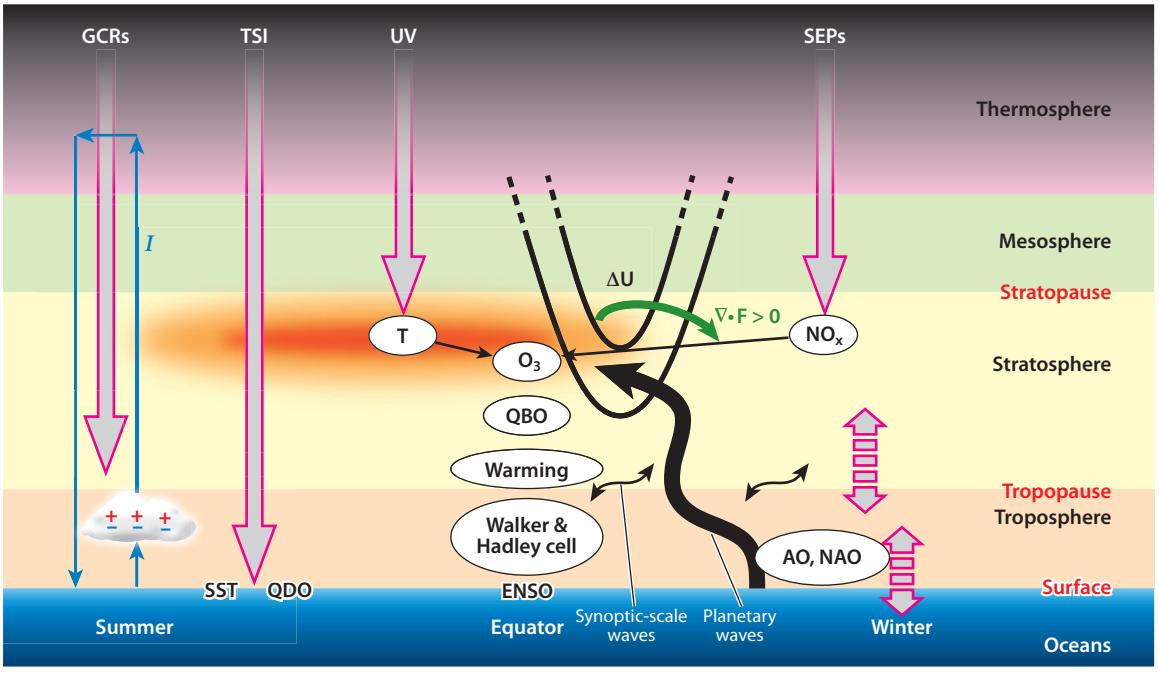

Figure 14

Schematic indicating mechanisms whereby variations in solar activity may influence the climate. Solar changes are via total solar irradiance (TSI), UV irradiance, solar energetic particles (SEPs) and Galactic cosmic rays (GCRs). Reprinted from Gray et al. (2010). Abbreviations: ENSO, El Niño Southern Oscillation; NAO, North Atlantic Oscillation; AO, Arctic Oscillation; QBO, Quasi-Biennial Oscillation; QDO, Quasi-Decadal Oscillation; SST, sea surface temperature; T, temperature.

by the Sun during storms and flares, impact the composition of the upper and middle atmosphere. The means whereby either of these effects may influence the climate (i.e., mean temperature, wind, precipitation) of the lower atmosphere are very uncertain. In this review, we concentrate on radiative processes and do not offer any further discussion of the effects of particles.

4.2.1. Solar radiative forcing of climate. The concept of RF is widely used (see e.g., Solomon et al. 2007) in analyzing and predicting the response of surface temperature to climate change factors, including increasing concentrations of greenhouse gases, higher atmospheric turbidity, changes in planetary albedo as well as changes in solar input. RF, in its most simple guise, is defined as the (hypothetical) instantaneous change in net radiation balance produced at the top of the atmosphere upon the introduction of a perturbing factor. It is useful because it has been shown [in experiments with general circulation models (GCMs) of the coupled atmosphere-ocean system] that the change in globally averaged surface temperature, at equilibrium, is linearly related to the RF value and is much less dependent on the specifics of the forcing factor. The constant of proportionality, called the climate sensitivity parameter, λ, has a value estimated to be in the range of 0.4–1.2 K W^{-1} m^2 with a best estimate of 0.6 K W^{-1} m^2 (see, e.g., Le Treut 2012) indicating that the equilibrated response of the global mean surface temperature to an RF of 1 W m^{-2} would be 0.6 K. We can use λ, together with estimates of time-varying TSI, to indicate the role of the Sun in global climate change. It is important to note, however, that there is not a 1:1 correspondence between changes in TSI and RF. This is because, while Earth projects an area of πR^2 to the Sun, the radiation is averaged over the $4\pi R^2$ of Earth's surface and, furthermore, only about 70% of

General circulation models (GCMs): models of the coupled atmosphere-ocean system

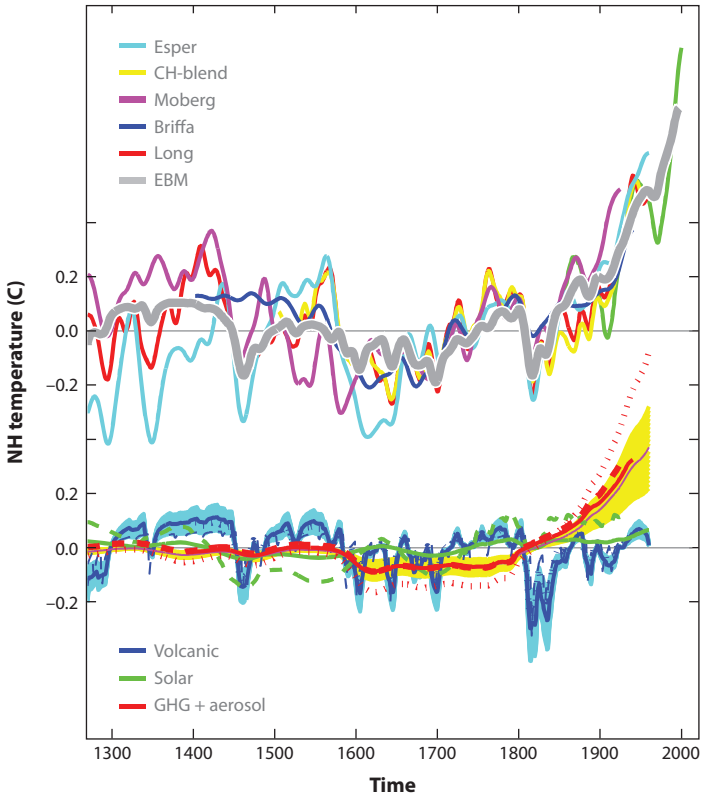

Figure 15

(*Top*) Global mean surface temperature since 1270 constructed from proxy data sets (*pink*, *red*, *cyan*, *blue*, and *yellow*) and from instrumental records, and calculated using an energy balance model (*gray*) scaled to best match the temperature reconstruction. (*Bottom*) Solid lines show estimates of the contributions from individual forcings—volcanic (*blue*), solar (*green*), and greenhouse gases and aerosols combined (*red*)—which give best fit to the red curve in the upper panel. Total is shown by the pink line with spread indicated by yellow area. Dotted (dashed) lines are the same but fit to the cyan (pink) curve in the upper panel. [G. Hegerl, personal communication; adapted from Solomon et al. (2007).]

solar radiation is absorbed with the other 30% reflected back to space. Thus a 1 W m^{-2} increase in TSI implies a RF of only 0.7/4 = 0.175 W m^{-2} and (taking $\lambda = 0.6$ K W^{-1} m^2) a global mean surface temperature increase of about 0.1 K.

A record of TSI may thus be used to indicate the role of the Sun in climate history, at least in a global average equilibrated context. A fundamental issue then is to establish the TSI record and, as discussed in Section 3.2, this is controversial. As an example, plausible estimates given for the difference between the Maunder minimum and the present probably lie in the range of 0.8–3.0 W m^{-2}, suggesting a solar-driven global temperature increase in the range of 0.08 to 0.30 K since the seventeenth century. The observed temperature difference is estimated at around 1 K so, on this basis, the Sun may have contributed 8–30% of the warming.

In order to achieve a more accurate estimate it is useful to employ time series of temperature records obtained from climate models with given external forcings. An example is presented for the past 800 years in **Figure 15**. This shows the temperature record constructed from proxy and instrumental data together with results derived from two climate models. The first is a 2D

(horizontal with realistic distribution of land and ocean) energy balance model, which estimates the temperature of the atmosphere and upper ocean, in response to time-varying RFs parameters, while taking account of slower heat exchange with the deep ocean. The second is a fully coupled atmosphere-ocean GCM. The models are driven by changes in greenhouse gases, tropospheric aerosol (sulfate, dust, and soot particles), stratospheric (volcanic) aerosol, as well as TSI. The lower curve shows the components of the temperature changes attributed to the individual forcings. The models suggest a TSI contribution at the low end of the range cited above, which is consistent with the results of statistical analyses such as those presented in **Figure 12** for the twentieth century. We conclude that though solar activity, and volcanism, are very likely to have contributed to variations in global (or hemispheric) average temperature over the millennium, including to the LIA and MCA, they cannot account for the sharp increase in warming since about 1960.

SST: sea surface temperature

4.2.2. A bottom-up mechanism for the influence of solar irradiance variability on climate. RF provides an indication of the global mean surface temperature response to variations in TSI but cannot explain the regional climate signals ascribed to solar variability, as outlined in Section 4.1. These cannot be driven directly by radiative processes but must be associated with changes in atmospheric circulation, and so to understand them it is necessary to look more deeply into the mechanisms involved.

The greatest intensity of solar radiation incident on Earth is in the tropics but most reaches the surface in the cloud-free subtropical regions. Over the oceans a large proportion of this radiant energy is used in evaporation. The resulting high-humidity air is advected into the tropics where it converges and rises, producing the deep cloud and heavy precipitation associated with that region. The main bottom-up mechanism for solar-climate links suggests that changes in the absorption of radiation in the clear-sky regions provide the driver (Cubasch et al. 1997). Greater irradiance would result in enhanced evaporation, moisture convergence, and precipitation. This would result in stronger Hadley and Walker circulations and stronger trade winds (driving greater upwelling in the eastern tropical Pacific Ocean), and colder SSTs, and thus the La Niña–like signal described in Section 4.1.1 above. There is some evidence for this effect being reproduced in GCM simulations of solar effects (Meehl et al. 2008), although the timing of the signal relative to the solar cycle peak remains contentious (Roy & Haigh 2012).

4.2.3. Spectral solar irradiance. The absorption of solar radiation by the atmosphere is determined by the spectral properties of the component gases and is, thus, a strong function of wavelength.

Figure 16*a* shows an example of how downward SSI, in the near-UV and visible bandwidths, depends on wavelength and on altitude within the atmosphere. As the radiation progresses downward, it is absorbed preferentially at wavelengths shorter than 350 nm and longer than 440 nm; **Figure 16*b*** indicates how the absorption of radiation translates into atmospheric heating rates. Absorption by molecular oxygen of radiation in the 200–242-nm region produces the oxygen atoms important in the production of ozone and also heats the stratopause region. Between 200 nm and 350 nm the radiation is responsible for the photodissociation of ozone and for strong radiative heating in the upper stratosphere and lower mesosphere. The ozone absorption bands, 440–800 nm, are much weaker, but because they absorb broadly across the peak of the solar spectrum, their energy deposition into the lower stratosphere is not insignificant.

Figure 17 shows the field of spectral irradiance, as in **Figure 16*a***, but for the difference between solar cycle maximum and minimum conditions, based on spectral variability of Lean (2000) (see Section 2.3). In these plots, the effects of changes in ozone concentration resulting from the enhanced solar irradiance are included. This means that the vertical penetration of the

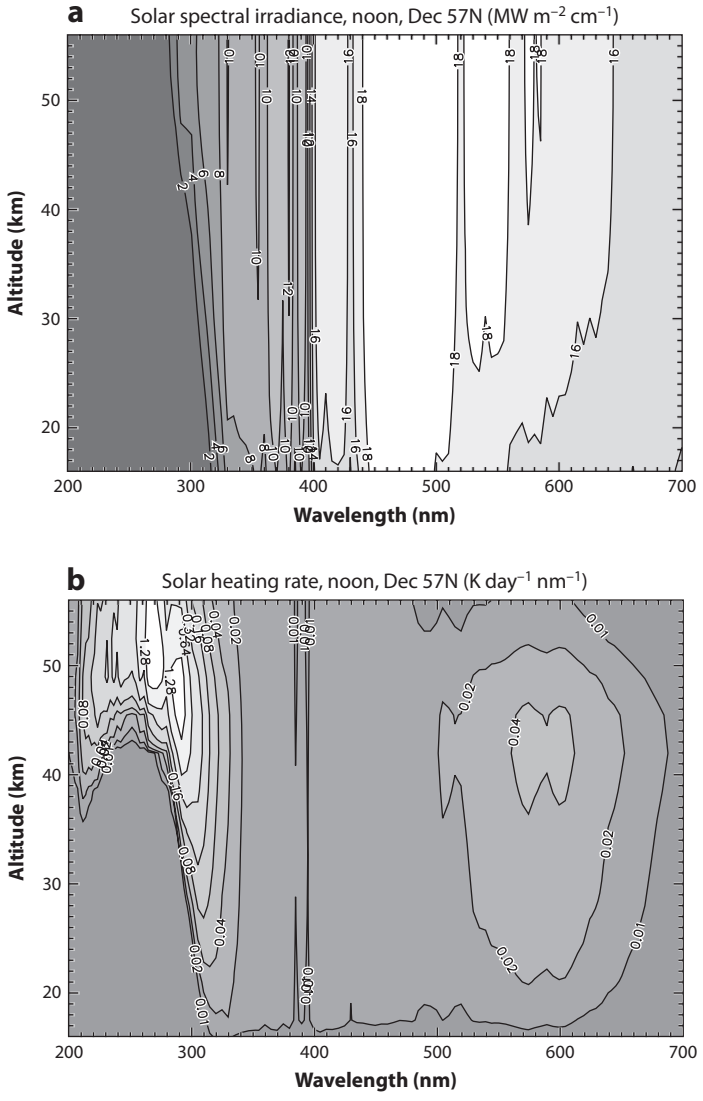

Figure 16

(*a*) Spectral solar irradiance at UV and visible wavelengths as a function of altitude within Earth's atmosphere [calculated using a coupled radiative-chemical-dynamical 2D model (Haigh 1994) for latitude 57°N, 21st December, noon, using spectral irradiance data at top of atmosphere for year 2000 from Lean (2000)]. (*b*) Solar spectral heating rate.

enhanced irradiance is not spectrally uniform because it depends on the ozone perturbation as well as the ozone absorption spectrum. Much of the increased irradiance penetrates to the surface, but at wavelengths less than 320 nm the increases in ozone result in lower values of irradiance throughout the stratosphere despite the increased insolation above. In similar fashion, at wavelengths in the 550–640-nm range, less radiation reaches the lower stratosphere. This effect is more marked at high solar zenith angles, and so leads to strong latitudinal gradients in the spectrally integrated irradiance in winter mid-latitudes. This gives an indication of the nonlinearity of the response in

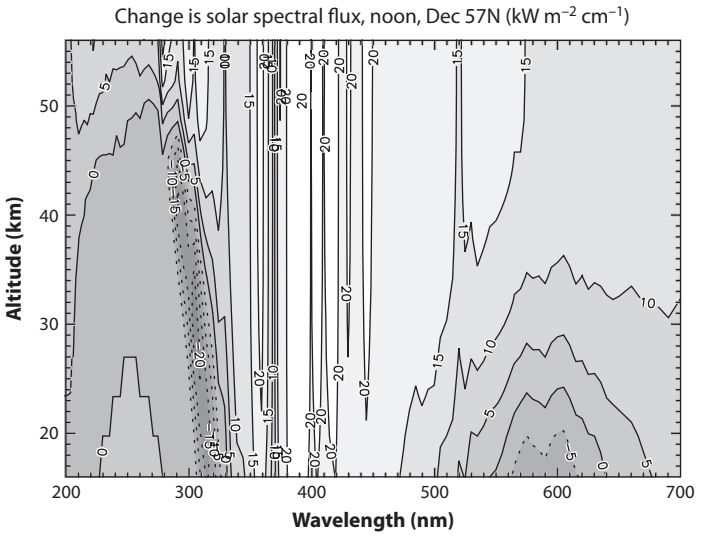

Figure 17

As in **Figure 16** but showing the difference in spectral irradiance between 2000 and 2007 (representing the maximum and minimum of the last solar activity cycle).

solar heating rates to variations in solar variability due to details of the photochemical response in ozone.

Recent satellite measurements (see Section 2.1) suggest that solar UV radiation varies by a much larger factor than assumed in **Figure 17**, whereas even the sign of the change in radiation at visible wavelengths is uncertain (Harder et al. 2009; cf. Ermolli et al. 2013). These preliminary results significantly affect estimates of the changes in heating rates, temperature, and ozone fields and, if such a spectral variability were confirmed to be representative of solar cycle behavior, or, indeed, of longer timescales, it would raise questions concerning current understanding of the response to solar variability of the temperature and composition of the middle atmosphere and also solar RF of climate (Haigh et al. 2010). However, there is some doubt about the reality of the extreme spectral dependence of irradiance variations found by Harder et al. [2009; see DeLand & Cebula (2012), Ermolli et al. (2013) and Sections 2.1 and 2.3].

4.2.4. Dynamical effects in the stratosphere. Attempts to predict the response of the stratosphere to solar UV variability were first carried out using 2D chemistry transport models, such as were used to estimate the solar radiation fields in **Figures 16** and **17**. These predicted a solar cycle response with a peak warming of around 1 K near the stratopause and peak increases in ozone of around 2% at altitudes around 40 km, with perturbations in both temperature and ozone monotonically decreasing toward the tropopause (e.g., Garcia et al. 1984, Haigh 1994). They did not reproduce the more complex latitudinal and vertical gradients, i.e., the double peak structure in the stratosphere described above. This indicates that the ozone response, at least in the middle and lower stratosphere, is influenced by modifications to its transport brought about by solar-induced changes in atmospheric circulation. Furthermore, as the structure in the temperature signal is fundamentally related to the ozone response, it is unlikely that any simulation will satisfactorily reproduce the one without the other.

It has long been appreciated that variations in solar heating affect the dynamical structure of the middle atmosphere. Changes in the meridional temperature gradients influence the

ENSO: El Niño Southern Oscillation

zonal wind structure and, thus, the upward propagation of the planetary-scale waves that deposit momentum and drive the mean overturning circulation of the stratosphere. The changed wind structure then has a further effect on wave propagation, as represented in the schematic of **Figure 14**. With greater solar heating near the tropical stratopause, the stratospheric jets are stronger, the polar vortices less disturbed, and the overturning circulation weaker (Kodera & Kuroda 2002). This produces cooling in the polar lower stratosphere due to weaker descent and warming at low latitudes through weaker ascent. Thus in the lower stratosphere the tropics are warmer, and the poles cooler, than would result from radiative processes alone.

Models with fully interactive chemistry have been employed so that the imposed irradiance variations affect both the radiative heating and the ozone photolysis rates, allowing feedback between heating, circulation, and composition [see the review by Austin et al. (2008)]. These models are broadly able to simulate the observed vertical structure of the solar signal in ozone in the tropics, although there is no clear picture as to what factor is responsible for the lower stratospheric maximum. Candidates include time-varying SSTs, transient solar input, high vertical resolution in the models, and their ability to produce natural modes of variability such as the Quasi-Biennial Oscillation or ENSO.

4.2.5. A top-down mechanism for the influence of solar irradiance variability on climate. Although the bottom-up mechanism is entirely plausible, it is premised on very small fractional variations in TSI and awaits confirmation of details of the processes involved. The larger fractional changes in the UV radiation suggest an alternative route. Studies of the impact of varying UV in climate models in which SSTs have been fixed are at least qualitatively successful in simulating the tropospheric patterns of response to solar variability (Haigh 1996, 1999; Larkin, Haigh & Djavidnia 2000; Matthes et al. 2006; Shindell et al. 1999). For example, **Figure 18*c*,*d*** shows the zonal wind climatology and the solar cycle signal, respectively, from a multiple regression analysis of the NCEP (National Centers for Environmental Prediction) Reanalysis data set (**http://www.cdc.noaa.gov/**). The solar signal appears as an inverted horseshoe pattern in the troposphere, representing the poleward shift of the jets at solar maximum, as mentioned in Section 4.1.2. **Figure 18*a*,*b*** presents the same fields calculated with an atmosphere-only GCM in response to increasing solar UV radiation. In both analyses, the jets weaken and move poleward and both also produce (not shown) the broadened Hadley cells. The strength of the model signal is weaker than that seen in the observations but is strengthened when larger increases in stratospheric ozone are imposed. Consistent with this, the Hadley circulation response in coupled chemistry simulations (Shindell et al. 2006) have been linked to the additional heating introduced into the tropical upper troposphere and lower stratosphere by solar-induced ozone. The model studies clearly reveal a dynamical influence of changes in the stratosphere on the troposphere rather than a direct radiative effect.

More generally, a number of different studies have indicated that such a downward influence does take place. Analyses of observational data suggest a downward propagation of polar circulation anomalies in both the Northern and Southern Hemispheres. Model studies have also demonstrated a downward influence from Antarctic stratospheric ozone depletion on the circumpolar circulation in the Southern Hemisphere (Gillett & Thompson 2003) and from stratospheric temperature trends on the NAO (Scaife et al. 2005). These studies did not specifically address the impact of solar variability on climate, but they did suggest that the troposphere responds to perturbations initiated in the stratosphere. More recently, a study by Ineson et al. (2011), using a coupled atmosphere-ocean GCM, prescribed changes to solar UV as suggested by SORCE/SIM measurements (in the 200–320-nm range only) and produced a significant shift to a negative NAO pattern—colder

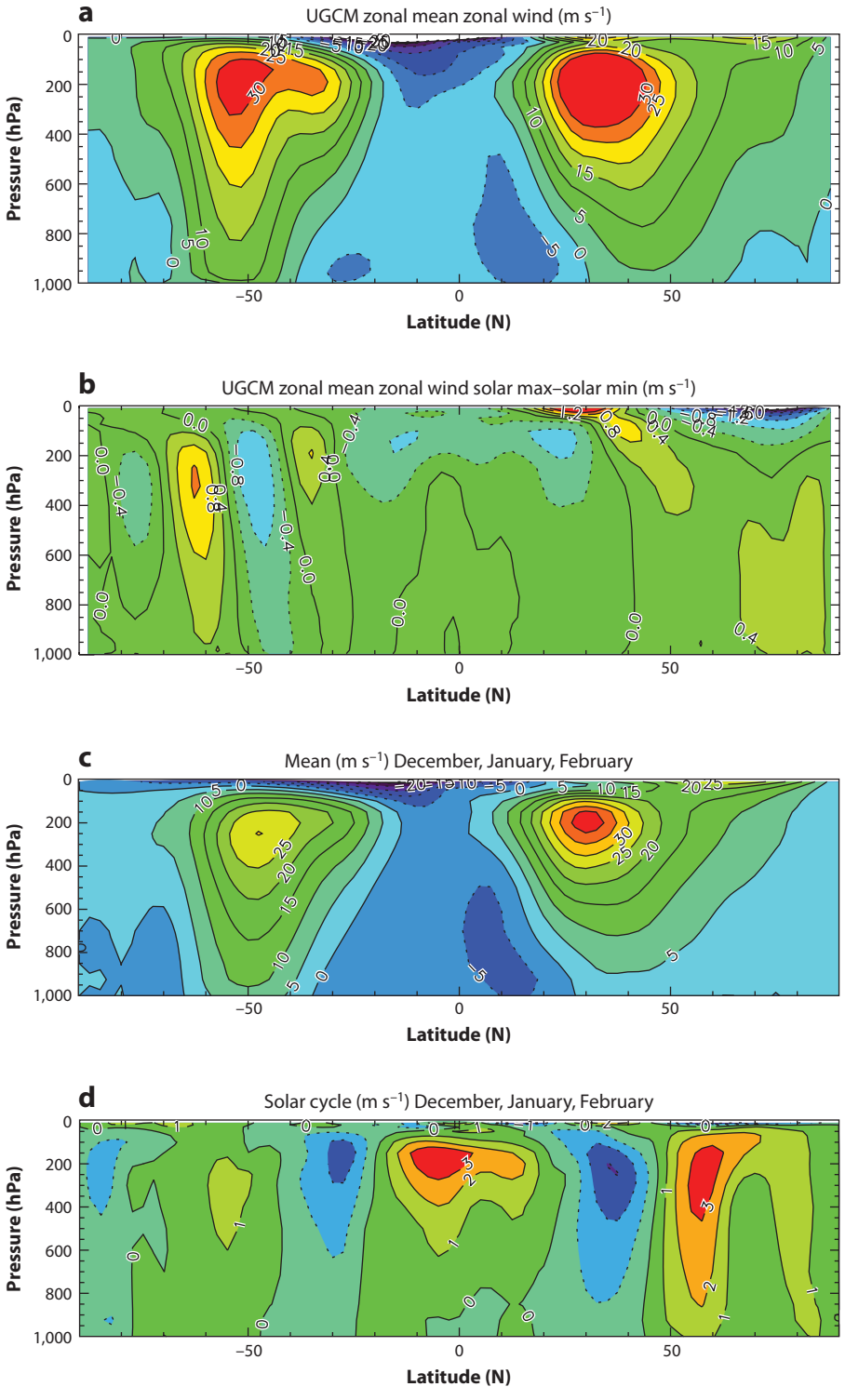

winters in Western Europe at lower solar activity—as suggested by observational records and presented in **Figure 13**.

There are many mechanisms proposed whereby the lower stratosphere may exert a dynamical influence on the troposphere [see reviews by Shepherd (2002), Haynes (2005), Gerber et al. (2012)]. These include a response of the mean meridional circulation to angular momentum forcing from above, modification of the transmission of upward-propagating planetary-scale waves, and feedbacks between changes in the mean-flow and tropospheric baroclinic eddies (weather systems).

Coupling between the Hadley circulation and the mid-latitude eddies may also play a key part. Studies with a simple climate model (Haigh, Blackburn & Day 2005), in which an anomalous heating was applied in the tropical lower stratosphere, found a zonal mean tropospheric response qualitatively similar to that observed in response to the solar cycle.

Further experiments have investigated the chain of causality involved in converting the stratospheric thermal forcing to a tropospheric climate signal (Haigh & Blackburn 2006; Simpson, Blackburn & Haigh 2009). They found that changes to the thermal structure of the lower stratosphere influenced the propagation of synoptic-scale waves, creating anomalies in eddy heat and momentum fluxes that drove changes in zonal wind and meridional circulation throughout the troposphere. These tropospheric changes then influenced the subsequent propagation of waves so as to reinforce the initial perturbations. They concluded that solar heating of the stratosphere may produce changes in the circulation of the troposphere even without any direct forcing below the tropopause and that the impact of the stratospheric changes on wave propagation is key to this effect.

Although details of the mechanisms involved are still not fully established, it is becoming increasingly clear that solar variability may influence the climate of the troposphere through processes whereby UV heating of the stratosphere indirectly influences the troposphere through dynamical coupling.

5. CONCLUSIONS

Space-based radiometers have recorded TSI since 1978 and have established that it varies at the 0.1% level over the solar cycle. Solar variability is a strong function of wavelength, increasing toward shorter wavelengths and, thus, reaching a factor of two in the Lyα line. Most of the irradiance variability of the Sun is produced by dark (sunspots, pores) and bright (magnetic elements forming faculae and the network) surface magnetic features, whose concentration changes over the solar cycle.

Various radiometers show many similarities in their results. Nonetheless, a few important differences are present that need to be removed before the solar influence on climate can be accurately estimated. One particularly relevant open issue is how strongly TSI changes on timescales longer

Figure 18

(*a*) Annual and zonal mean zonal wind as a function of latitude and pressure altitude from a climate model. (*b*) Difference in zonal mean zonal wind between solar maximum and minimum of the 11-year cycle calculated by imposing changes in UV in the model (Haigh 1999). (*c*) As in panel *a* but using data from the National Centers for Environmental Prediction (NCEP) data set. (*d*) Solar signal (max-min) in the NCEP data set derived using multiple linear regression (Haigh 2003). Abbreviation: UGCM, UK Universities' Global Atmospheric Modelling Programme General Circulation Model.

than the solar cycle. Composites of TSI records from different instruments put together by different researchers display a broad variety of behaviors. Models of TSI show the best agreement with the so-called PMOD composite. In spite of this general consensus between models, the model-based estimates of the rise in TSI since the Maunder minimum differ by almost a factor of four, with correspondingly different effects on the outputs of climate models. Aside from this scaling issue, the models do agree relatively well (e.g., in their temporal behavior) so that the irradiance can now be reconstructed over the whole Holocene, covering multiple grand minima and maxima of solar activity.

Another bone of contention is the behavior of the spectral irradiance over the solar cycle. The modeled spectral irradiance at all wavelengths, except around the opacity minimum region in the IR, varies in phase with the solar cycle and with the TSI. The SIM instrument on the SORCE satellite, by contrast, finds an antiphase behavior over large parts of the visible wavelength range and a UV variability larger by a factor of 2–6 than that found by any model that also reproduces TSI. There are hints that the problem may lie with the SORCE SSI data.

There is growing evidence that changes in solar irradiance affect Earth's middle and lower atmosphere. At higher levels of activity, the stratosphere is warmer throughout the tropics, associated with higher concentrations of ozone. At such times, patterns consistent with an expansion of the tropical Hadley circulations are established. At the surface, a more active Sun is associated with a more positive phase of North Atlantic Oscillation, especially in winter, and a north-westward shift of the main surface pressure features in the North Pacific.

Globally the mean surface temperature varies in phase with solar activity. Over the past few solar cycles, for which measurements of TSI are available, the small amplitude of this variation is consistent with what would be deduced from RF arguments (of order 0.1 K for a 1-W m^{-2} change in TSI). On longer timescales, while the in-phase relationship broadly persists back into the past, the amplitude is less easy to associate directly with RF because of the large uncertainties in TSI variations. However, it is virtually impossible to assign the global warming of the past half century to variations in solar irradiance alone, using either statistical or physical methods.

In understanding the distribution of the solar signals throughout the troposphere and across Earth's surface, it is necessary to invoke processes other than direct radiative heating alone. The most plausible scenarios involve changes in circulation, winds, etc., in response to absorption of visible radiation at the surface and/or UV radiation in the stratosphere. Two main mechanisms have been proposed: the bottom-up mechanism relying on absorption of mainly visible radiation at the surface and the top-down mechanism relying on absorption of UV radiation in the stratosphere. The first of these is dependent on enhanced heating and evaporation at the cloud-free subtropical ocean surface with impacts on the intertropical convergence zone and tropical circulations in the atmosphere and ocean. The second involves changes in the thermal structure of the stratosphere with dynamical coupling downward. At present, the theory of, and evidence for, the stratospheric route is better developed, although uncertainty in solar UV variability leaves scope for this to be revised. The two routes are not mutually exclusive and may operate synergistically.

In summary, considerable progress has been made in the past decade on the topic of solar irradiance variability and its influence on climate, but new data and models have also revealed new inconsistencies that will provide a challenge for the future. It is an interdisciplinary field that has reverberations well beyond astrophysics, and considerable effort will be required to overcome the challenges ahead.

FUTURE ISSUES

Further advances in understanding solar variability and its influence on climate will benefit from continuing acquisition of high-quality measurements of solar and climate variables and the development of models including all the relevant processes. The next generation of solar irradiance models will make use of model atmospheres obtained from three-dimensional magnetohydrodynamic simulations allowing a more realistic representation of the spectral properties of magnetic features.

DISCLOSURE STATEMENT

The authors are not aware of any affiliations, memberships, funding, or financial holdings that might be perceived as affecting the objectivity of this review.

ACKNOWLEDGMENTS

We thank G. Kopp, W. Ball, Y.C. Unruh, and I. Usoskin for providing **Figures 1**; **2** and **6**; **7**; and **9**, respectively. We are grateful to J. Lean, A. Shapiro, and F. Steinhilber for providing or making public their TSI reconstructions (used in **Figure 10**), as well as to L. Floyd, J. Harder, M. Snow, and T. Woods for the spectral irradiance data (shown in **Figure 3**). J.D.H. would like to acknowledge the many colleagues who contributed to the Solar Influences on Climate Consortium funded by the UK Natural Environment Research Council. This work has been partially supported by the WCU grant (No. R31–10016) funded by the Korean Ministry of Education, Science and Technology.

LITERATURE CITED

Abreu JA, Beer J, Steinhilber F, Tobias SM, Weiss NO. 2008. *Geophys. Res. Lett.* 352:L20109
Arge CN, Hildner E, Pizzo VJ, Harvey JW. 2002. *J. Geophys. Res.* 107(A10):SSH16-1–18
Austin J, Tourpali K, Rozanov E, Akiyoshi H, Bekki S, et al. 2008. *J. Geophys. Res.* 113:D11306
Baglin A, Auvergne M, Barge P, Buey JT, Catala C, et al. 2002. In *Stellar Structure and Habitable Planet Finding*, ed. B Battrick, F Favata, IW Roxburgh, D Galadí, ESA SP-485:17–24. Noordwijk: ESA Publicat.
Ball WT. 2012. *Observations and Modelling of Total and Spectral Solar Irradiance.* PhD thesis. Imperial College London, UK
Ball WT, Unruh YC, Krivova NA, Solanki SK, Harder JW. 2011. *Astron. Astrophys.* 530:A71
Ball WT, Unruh YC, Krivova NA, Solanki SK, Wenzler T, et al. 2012. *Astron. Astrophys.* 541:A27
Balmaceda LA, Solanki SK, Krivova NA, Foster S. 2009. *J. Geophys. Res.* 114:A07104
Berger TE, Schrijver CJ, Shine RA, Tarbell TD, Title AM, Scharmer G. 1995. *Ap. J.* 454:531
Bolduc C, Charbonneau P, Dumoulin V, Bourqui MS, Crouch AD. 2012. *Sol. Phys.* 279:383–409
Borucki WJ, Koch DG, Basri GB, Caldwell DA, Caldwell JF, et al. 2003. In *Scientific Frontiers in Research on Extrasolar Planets*, ed. D Deming, S Seager, *ASP Conf. Ser.* 294:427. San Francisco: ASP
Brönnimann S, Annis JL, Vogler C, Jones PD. 2007. *Geophys. Res. Lett.* 34:22805
Brueckner GE, Edlow KL, Floyd LE, Lean JL, Vanhoosier ME. 1993. *J. Geophys. Res.* 98:10695–711
Carlsson M, Stein RF. 1997. *Ap. J.* 481:500
Carlsson M, Stein RF, Nordlund Å, Scharmer GB. 2004. *Ap. J. Lett.* 610:L137–40
Cebula RP, DeLand MT, Schlesinger BM. 1992. *J. Geophys. Res.* 97:11613–20
Chapman GA, Cookson AM, Dobias JJ. 1996. *J. Geophys. Res.* 101:13541–48
Chapman GA, Cookson AM, Preminger DG. 2012. *Sol. Phys.* 276:35–41
Charbonneau P. 2010. *Living Rev. Sol. Phys.* 7:3

Charbonnel C, Däppen W, Schaerer D, Bernasconi PA, Maeder A, et al. 1999. *Astron. Astrophys. Suppl.* 135:405–13
Christoforou P, Hameed S. 1997. *Geophys. Res. Lett.* 24:293–96
Crucifix M, Loutre MF, Berger A. 2006. *Space Sci. Rev.* 125:213–26
Cubasch U, Voss R, Hegerl GC, Waszkewitz J, Crowley TJ. 1997. *Clim. Dyn.* 13:757–67
DeLand MT, Cebula RP. 2008. *J. Geophys. Res.* 113:A11103
DeLand MT, Cebula RP. 2012. *J. Atmos. Sol.-Terr. Phys.* 77:225–34
de Wijn AG, Stenflo JO, Solanki SK, Tsuneta S. 2009. *Space Sci. Rev.* 144:275–315
Dewitte S, Crommelynck D, Joukoff A. 2004. *J. Geophys. Res.* 109:2102
Dewitte S, Crommelynck D, Mekaoui S, Joukoff A. 2004. *Sol. Phys.* 224:209–16
Domingo V, Ermolli I, Fox P, Fröhlich C, Haberreiter M, et al. 2009. *Space Sci. Rev.* 145:337–80
Eddy JA. 1976. *Science* 192:1189–202
Ermolli I, Berrilli F, Florio A. 2003. *Astron. Astrophys.* 412:857–64
Ermolli I, Criscuoli S, Giorgi F. 2011. *Contrib. Astron. Obs. Skalnate Pleso* 41:73–84
Ermolli I, Matthes K, Dudok de Wit T, Krivova NA, Tourpali K, et al. 2013. *Atmos. Chem. Phys.* 13:3945–77
Ermolli I, Solanki SK, Tlatov AG, Krivova NA, Ulrich RK, Singh J. 2009. *Ap. J.* 698:1000–9
Fawzy DE, Cuntz M, Rammacher W. 2012. *MNRAS* 426:1916–27
Fehlmann A, Kopp G, Schmutz W, Winkler R, Finsterle W, Fox N. 2012. *Metrologia* 49:34
Field CV, Schmidt GA, Koch D, Salyk C. 2006. *J. Geophys. Res.* 111:15107
Fligge M, Solanki SK, Unruh YC. 2000. *Astron. Astrophys.* 353:380–88
Floyd LE, Cook JW, Herring LC, Crane PC. 2003. *Adv. Space Res.* 31:2111–20
Fontenla J, White OR, Fox PA, Avrett EH, Kurucz RL. 1999. *Ap. J.* 518:480–99
Fontenla JM, Curdt W, Haberreiter M, Harder J, Tian H. 2009. *Ap. J.* 707:482–502
Fontenla JM, Harder J, Livingston W, Snow M, Woods T. 2011. *J. Geophys. Res.* 116:20108
Fontenla JM, Harder J, Rottman G, Woods TN, Lawrence GM, Davis S. 2004. *Ap. J. Lett.* 605:L85–88
Foster S. 2004. *Reconstruction of solar irradiance variations for use in studies of global climate change: Application of recent SOHO observations with historic data from the Greenwich observatory*. PhD thesis. Univ. Southampton, Sch. Phys. Astron.
Foukal P, Lean J. 1986. *Ap. J.* 302:826–35
Foukal P, Milano L. 2001. *Geophys. Res. Lett.* 28:883–86
Frame THA, Gray LJ. 2010. *J. Clim.* 23:2213–22
Fröhlich C. 2006. *Space Sci. Rev.* 125:53–65
Fröhlich C. 2009. *Astron. Astrophys.* 501:L27–30
Fröhlich C. 2012. *Surv. Geophys.* 33:453–73
Fröhlich C, Brusa RW. 1981. *Sol. Phys.* 74:209–15
Fröhlich C, Lean J. 2004. *Astron. Astrophys. Rev.* 12:273–320
Fröhlich C, Romera J, Roth H, Wehrli C, Andersen BN, et al. 1981. *Sol. Phys.* 162:101–28
Garcia RR, Solomon S, Roble RG, Rusch DW. 1984. *Planet. Space Sci.* 32:411–23
Gerber EP, Butler A, Calvo N, Charlton-Perez A, Giorgetta M, et al. 2012. *Bull. Am. Meteorol. Soc.* 93:845–59
Gillett NP, Thompson DWJ. 2003. *Science* 302:273–75
Gray LJ, Beer J, Geller M, Haigh JD, Lockwood M, et al. 2010. *Rev. Geophys.* 48:4001
Gray LJ, Beer J, Geller M, Haigh JD, Lockwood M, et al. 2012. *Rev. Geophys.* 50:RG1006
Grossmann-Doerth U, Knoelker M, Schuessler M, Solanki SK. 1994. *Astron. Astrophys.* 285:648–54
Hagenaar HJ, Schrijver CJ, Title AM. 2003. *Ap. J.* 584:1107–19
Haigh JD. 1994. *Nature* 370:544–46
Haigh JD. 1996. *Science* 272:981–84
Haigh JD. 1999. *J. Atmos. Sol.-Terr. Phys.* 61:63–72
Haigh JD. 2003. *Philos. Trans. R. Soc. Lond. A* 361:95–111
Haigh JD. 2007. *Living Rev. Sol. Phys.* 4:2
Haigh JD, Blackburn M. 2006. *Space Sci. Rev.* 125:331–44
Haigh JD, Blackburn M, Day R. 2005. *J. Clim.* 18:3672–85
Haigh JD, Lockwood M, Giampapa MS, eds. 2005. *The Sun, Solar Analogs and the Climate, Saas-Fee Advanced Course* 34. Berlin: Springer

Haigh JD, Winning AR, Toumi R, Harder JW. 2010. *Nature* 467:696–99
Hall JC, Henry GW, Lockwood GW, Skiff BA, Saar SH. 2009. *Astron. J.* 138:312–22
Hall JC, Lockwood GW. 2004. *Ap. J.* 614:942–46
Harder J, Lawrence G, Fontenla J, Rottman G, Woods T. 2005. *Sol. Phys.* 230:141–67
Harder JW, Fontenla JM, Pilewskie P, Richard EC, Woods TN. 2009. *Geophys. Res. Lett.* 36:L07801
Harvey KL. 1992. In *The Solar Cycle*, ed. KL Harvey. *ASP Conf. Ser.* 27:335–67. San Francisco: ASP
Harvey KL. 1993. In *The Magnetic and Velocity Fields of Solar Active Regions, IAU Colloq. 141*, ed. H Zirin, A Guoxiang, H Wang. *ASP Conf. Ser.* 46:488. San Francisco: ASP
Harvey KL. 1994. In *Solar Surface Magnetism*, ed. RJ Rutten, CJ Schrijver, pp. 347–63. Dordrecht: Kluwer
Hathaway DH. 2010. *Living Rev. Sol. Phys.* 7:1
Haynes P. 2005. *Annu. Rev. Fluid Mech.* 37:263–93
Hegerl GC, Crowley TJ, Allen M, Hyde WT, Pollack HN, et al. 2007. *J. Clim.* 20:650–66
Hickey JR, Stowe LL, Jacobowitz H, Pellegrino P, Maschhoff RH, et al. 1980. *Science* 208:281–83
Hoyt DV, Kyle HL, Hickey JR, Maschhoff RH. 1992. *J. Geophys. Res.* 97:51–63
Hoyt DV, Schatten KH. 1998. *Sol. Phys.* 179:189–219
Ineson S, Scaife AA, Knight JR, Manners JC, Dunstone NJ, et al. 2011. *Nat. Geosci.* 4:753–57
Joshi J, Pietarila A, Hirzberger J, Solanki SK, Aznar Cuadrado R, Merenda L. 2011. *Ap. J. Lett.* 734:L18
Judge PG, Lockwood GW, Radick RR, Henry GW, Shapiro AI, et al. 2012. *Astron. Astrophys.* 544:A88
Keller CU, Schüssler M, Vögler A, Zakharov V. 2004. *Ap. J. Lett.* 607:L59–62
Kirkby J, Curtius J, Almeida J, Dunne E, Duplissy J, et al. 2011. *Nature* 476:429–33
Knudsen MF, Riisager P, Donadini F, Snowball I, Muscheler R, et al. 2008. *Earth Planet. Sci. Lett.* 272:319–29
Kodera K. 2004. *Geophys. Res. Lett.* 31:L24209
Kodera K, Kuroda Y. 2002. *J. Geophys. Res.* 107(D24):ACL 5–1–12
Kopp G, Fehlmann A, Finsterle W, Harber D, Heuerman K, Willson R. 2012. *Metrologia* 49:29
Kopp G, Lawrence G, Rottman G. 2005. *Sol. Phys.* 230:129–39
Kopp G, Lean JL. 2011. *Geophys. Res. Lett.* 38:L01706
Korte M, Constable CG. 2005. *Earth Planet. Sci. Lett.* 236:348–58
Krivova NA, Balmaceda L, Solanki SK. 2007. *Astron. Astrophys.* 467:335–46
Krivova NA, Solanki SK. 2012. In *Climate and Weather of the Sun-Earth System* (*CAWSES*): *Highlights from a Priority Program*, ed. FJ Lübken, pp. 19–38. Dordrecht, The Netherlands: Springer
Krivova NA, Solanki SK, Fligge M, Unruh YC. 2003. *Astron. Astrophys.* 399:L1–4
Krivova NA, Solanki SK, Floyd L. 2006. *Astron. Astrophys.* 452:631–39
Krivova NA, Solanki SK, Unruh YC. 2011. *J. Atmos. Sol.-Terr. Phys.* 73:223–34
Krivova NA, Solanki SK, Wenzler T. 2009. *Geophys. Res. Lett.* 36:L20101
Krivova NA, Solanki SK, Wenzler T, Podlipnik B. 2009. *J. Geophys. Res.* 114(D1):16
Krivova NA, Vieira LEA, Solanki SK. 2010. *J. Geophys. Res.* 115:A12112
Kuhn JR, Bush RI, Scheick X, Scherrer P. 1998. *Nature* 392:155–57
Kurucz R. 1993. *ATLAS9 Stellar Atmosphere Programs and 2 km/s grid. Kurucz CD-ROM No. 13.* Cambridge, MA: Smithson. Astrophys. Obs.
Labitzke K. 2001. *Meteorol. Z.* 10:83–90
Lagg A, Solanki SK, Riethmüller TL, Martínez Pillet V, Schüssler M, et al. 2010. *Ap. J. Lett.* 723:L164–68
Larkin A, Haigh JD, Djavidnia S. 2000. *Space Sci. Rev.* 94:199–214
Lean J. 1997. *Annu. Rev. Astron. Astrophys.* 35:33–67
Lean J. 2000. *Geophys. Res. Lett.* 27:2425–28
Lean J, Rottman G, Harder J, Kopp G. 2005. *Sol. Phys.* 230:27–53
Lean J, Skumanich A, White O. 1992. *Geophys. Res. Lett.* 19:1595–98
Lean JL, DeLand MT. 2012. *J. Clim.* 25:2555–60
Lean JL, Rind DH. 2008. *Geophys. Res. Lett.* 35:L18701
Lean JL, Rottman GJ, Kyle HL, Woods TN, Hickey JR, Puga LC. 1997. *J. Geophys. Res.* 102:29939–56
Lee RB III, Gibson MA, Wilson RS, Thomas S. 1995. *J. Geophys. Res.* 100:1667–75
Le Treut H. 2012. *Surv. Geophys.* 33:723–31
Lockwood M. 2005. See Haigh, Lockwood & Giampapa. 2005, pp. 109–306
Lockwood M. 2009. *Proc. R. Soc. Lond. A* 466:303–29

Lockwood M, Rouillard AP, Finch ID. 2009. *Ap. J.* 700:937–44
Lockwood M, Stamper R. 1999. *Geophys. Res. Lett.* 26:2461–64
Lockwood M, Stamper R, Wild MN. 1999. *Nature* 399:437–39
Marsh ND, Svensmark H. 2000. *Phys. Rev. Lett.* 85:5004–7
Matthes K, Kuroda Y, Kodera K, Langematz U. 2006. *J. Geophys. Res.* 111:D06108
Meehl GA, Arblaster JM, Branstator G, van Loon H. 2008. *J. Clim.* 21:2883–97
Mendoza B. 1997. *Ap. J.* 483:523–26
Mordvinov AV, Makarenko NG, Ogurtsov MG, Jungner H. 2004. *Sol. Phys.* 224:247–53
Morrill JS, Floyd L, McMullin D. 2011. *Sol. Phys.* 269:253–67
Mowlavi N, Eggenberger P, Meynet G, Ekström S, Georgy C, et al. 2012. *Astron. Astrophys.* 541:A41
Muller R, Roudier T. 1984. *Sol. Phys.* 94:33–47
Musielak ZE, Ulmschneider P. 2003. *Astron. Astrophys.* 400:1057–64
Oster L, Schatten KH, Sofia S. 1982. *Ap. J.* 256:768–73
Pagaran J, Weber M, Burrows J. 2009. *Ap. J.* 700:1884–95
Paillard D. 2001. *Rev. Geophys.* 39:325–46
Pap JM, Fox P, Fröhlich C, Hudson HS, Kuhn J, et al. eds. 2004. *Solar Variability and Its Effects on Climate. Geophys. Monogr.* 141. Washington, DC: Am. Geophys. Union
Preminger DG, Walton SR, Chapman GA. 2002. *J. Geophys. Res.* 107(A11):1354
Rast MP, Meisner RW, Lites BW, Fox PA, White OR. 2001. *Ap. J.* 557:864–79
Rempel M, Schlichenmaier R. 2011. *Living Rev. Sol. Phys.* 8:3
Rempel M, Schüssler M, Cameron RH, Knölker M. 2009. *Science* 325:171–74
Rezaei R, Schlichenmaier R, Beck CAR, Bruls JHMJ, Schmidt W. 2007. *Astron. Astrophys.* 466:1131–44
Riethmüller TL, Solanki SK, Martínez Pillet V, Hirzberger J, Feller A, et al. 2010. *Ap. J. Lett.* 723:L169–74
Rottman GJ, Woods TN, Sparn TP. 1993. *J. Geophys. Res.* 98(D6):10667–77
Roy I, Haigh JD. 2010. *Atmos. Chem. Phys.* 10:3147–53
Roy I, Haigh JD. 2012. *J. Atmos. Sci.* 69:1446–51
Sackmann IJ, Boothroyd AI, Kraemer KE. 1993. *Ap. J.* 418:457
Sánchez Almeida J, Márquez I, Bonet JA, Domínguez Cerdeña I, Muller R. 2004. *Ap. J. Lett.* 609:L91–94
Scaife AA, Knight JR, Vallis GK, Folland CK. 2005. *Geophys. Res. Lett.* 32:L18715
Scharmer GB, Henriques VMJ, Kiselman D, de la Cruz Rodríguez J. 2011. *Science* 333:316–19
Schrijver CJ, Cote J, Zwaan C, Saar SH. 1989. *Ap. J.* 337:964–76
Schrijver CJ, Livingston WC, Woods TN, Mewaldt RA. 2011. *Geophys. Res. Lett.* 38:L06701
Schüssler M, Vögler A. 2006. *Ap. J. Lett.* 641:L73–76
Seleznyov AD, Solanki SK, Krivova NA. 2011. *Astron. Astrophys.* 532:A108
Shapiro AI, Schmutz W, Rozanov E, Schoell M, Haberreiter M, et al. 2011. *Astron. Astrophys.* 529:A67
Shapiro AI, Schmutz W, Schoell M, Haberreiter M, Rozanov E. 2010. *Astron. Astrophys.* 517:A48
Shaviv NJ. 2002. *Phys. Rev. Lett.* 89:051102
Sheeley NR Jr. 1969. *Sol. Phys.* 9:347–57
Shepherd TG. 2002. *J. Meteorol. Soc. Jpn.* 80:769–92
Shindell D, Rind D, Balachandran N, Lean J, Lonergan P. 1999. *Science* 284:305–8
Shindell DT, Faluvegi G, Miller RL, Schmidt GA, Hansen JE, Sun S. 2006. *Geophys. Res. Lett.* 33:L24706
Simpson IR, Blackburn M, Haigh JD. 2009. *J. Atmos. Sci.* 66:1347–65
Skumanich A, Smythe C, Frazier EN. 1975. *Ap. J.* 200:747–64
Smith EVP, Gottlieb DM. 1974. *Space Sci. Rev.* 16:771–802
Snow M, McClintock WE, Rottman G, Woods TN. 2005. *Sol. Phys.* 230:295–324
Sofia S, Li LH. 2001. *J. Geophys. Res.* 106:12969–74
Solanki SK. 1993. *Space Sci. Rev.* 63:1–2
Solanki SK. 2003. *Astron. Astrophys. Rev.* 11:153–286
Solanki SK, Finsterle W, Rüedi I, Livingston W. 1999. *Astron. Astrophys.* 347:L27–30
Solanki SK, Fligge M. 2000. *Space Sci. Rev.* 94:127–38
Solanki SK, Krivova NA. 2011. *Science* 334:916–17
Solanki SK, Krivova NA, Wenzler T. 2005. *Adv. Space Res.* 35:376–83
Solanki SK, Schüssler M, Fligge M. 2000. *Nature* 408:445–47

Solanki SK, Schüssler M, Fligge M. 2002. *Astron. Astrophys.* 383:706–12
Solanki SK, Unruh YC. 1998. *Astron. Astrophys.* 329:747–53
Solanki SK, Usoskin IG, Kromer B, Schüssler M, Beer J. 2004. *Nature* 431:1084–87
Sol. Influ. Data Anal. Cent. (SIDC). 2011. **http://sidc.oma.be/**
Solomon S, Qin D, Manning M, Chen Z, Marquis M, et al. eds. 2007. *Climate Change 2007: The Physical Science Basis. Contribution of Working Group I to the Fourth Assessment Report of the Intergovernmental Panel on Climate Change*. Cambridge, UK/New York: Cambridge Univ. Press
Soon WWH, Yaskell SH. 2003. *The Maunder Minimum: The Variable Sun-Earth Connection.* River Edge, NJ: World Sci.
Spruit H. 2000. *Space Sci. Rev.* 94:113–26
Spruit HC. 1976. *Sol. Phys.* 50:269–95
Spruit HC. 1982a. *Astron. Astrophys.* 108:348–55
Spruit HC. 1982b. *Astron. Astrophys.* 108:356–60
Stein RF. 2012. *Living Rev. Sol. Phys.* 9:4
Steinhilber F, Abreu JA, Beer J. 2008. *Ap. Space Sci. Trans.* 4:1–6
Steinhilber F, Abreu JA, Beer J, Brunner I, Christl M, et al. 2012. *Proc. Natl. Acad. Sci. USA* 109:5967–71
Steinhilber F, Beer J, Fröhlich C. 2009. *Geophys. Res. Lett.* 36:L19704
Stuiver M. 1991. *Quat. Res.* 35:1–24
Stuiver M, Braziunas TF. 1989. *Nature* 338:405–8
Svensmark H. 2012. *MNRAS* 423:1234–53
Thuillier G, Deland M, Shapiro A, Schmutz W, Bolsée D, Melo SML. 2012. *Sol. Phys.* 277:245–66
Thuillier G, Floyd L, Woods TN, Cebula R, Hilsenrath E, et al. 2004. *Adv. Sp. Res.* 34:256–61
Thuillier G, Foujols T, Bolsée D, Gillotay D, Hersé M, et al. 2009. *Sol. Phys.* 257:185–213
Thuillier G, Hersé M, Labs D, Foujols T, Peetermans W, et al. 2003. *Sol. Phys.* 214:1–22
Unruh YC, Ball WT, Krivova NA. 2012. *Surv. Geophys.* 33(3–4):475–81
Unruh YC, Solanki SK, Fligge M. 1999. *Astron. Astrophys.* 345:635–42
Uppala SM, Kallberg PW, Simmons AJ, Andrae U, Bechtold VD, et al. 2005. *Q. J. R. Meteorol. Soc.* 131:2961–3012
Usoskin IG. 2008. *Living Rev. Sol. Phys.* 5:3
Usoskin IG, Horiuchi K, Solanki S, Kovaltsov GA, Bard E. 2009. *J. Geophys. Res.* 114:3112
Usoskin IG, Mursula K, Solanki S, Schüssler M, Alanko K. 2004. *Astron. Astrophys.* 413:745–51
Usoskin IG, Mursula K, Solanki SK, Schüssler M, Kovaltsov GA. 2002. *J. Geophys. Res.* 107(A11):1374
Usoskin IG, Solanki SK, Kovaltsov GA. 2007. *Astron. Astrophys.* 471:301–9
Usoskin IG, Solanki SK, Kovaltsov GA. 2012. In *Comparative Magnetic Minima: Characterizing Quiet Times in the Sun and Stars*, *Proc. IAU Symp. 286*, ed. CH Mandrini, DF Webb, pp. 372–82. Cambridge, UK: Cambridge Univ. Press
Usoskin IG, Solanki SK, Schüssler M, Mursula K, Alanko K. 2003a. *Phys. Rev. Lett.* 91:211101–4
Usoskin IG, Solanki SK, Taricco C, Bhandari N, Kovaltsov GA. 2006. *Astron. Astrophys.* 457:L25–28
van Loon H, Meehl GA, Shea DJ. 2007. *J. Geophys. Res.* 112:D02108
Vaquero JM, Gallego MC, Usoskin IG, Kovaltsov GA. 2011. *Ap. J. Lett.* 731:L24–27
Vieira LEA, Solanki SK. 2010. *Astron. Astrophys.* 509:A100
Vieira LEA, Solanki SK, Krivova NA, Usoskin I. 2011. *Astron. Astrophys.* 531:A6
Viereck R, Puga L, McMullin D, Judge D, Weber M, Tobiska WK. 2001. *Geophys. Res. Lett.* 28:1343–46
Vögler A, Shelyag S, Schüssler M, Cattaneo F, Emonet T, Linde T. 2005. *Astron. Astrophys.* 429:335–51
Waldmeier M. 1939. *Astron. Mitt. Eidgenössis. Sternwarte Zür.* 14:439–50
Wang YM, Lean JL, Sheeley NR. 2005. *Ap. J.* 625:522–38
Wang YM, Sheeley NR Jr, Rouillard AP. 2006. *Ap. J.* 644:638–45
Wenzler T, Solanki SK, Krivova NA. 2009. *Geophys. Res. Lett.* 36:L11102
Wenzler T, Solanki SK, Krivova NA, Fröhlich C. 2006. *Astron. Astrophys.* 460:583–95
Willson RC. 1997. *Science* 277:1963–65
Willson RC, Gulkis S, Janssen M, Hudson HS, Chapman GA. 1981. *Science* 211:700–2
Willson RC, Hudson HS. 1988. *Nature* 332:810–12

Willson RC, Mordvinov AV. 2003. *Geophys. Res. Lett.* 30:1199
Wolff CL, Hickey JR. 1987. *Science* 235:1631–33
Woods TN, Chamberlin PC, Harder JW, Hock RA, Snow M, et al. 2009. *Geophys. Res. Lett.* 36:1101
Woods TN, Prinz DK, Rottman GJ, London J, Crane PC, et al. 1996. *J. Geophys. Res.* 101(D6):9541–69
Woods TN, Tobiska WK, Rottman GJ, Worden JR. 2000. *J. Geophys. Res.* 105:27195–215
Woollings T, Lockwood M, Masato G, Bell C, Gray L. 2010. *Geophys. Res. Lett.* 37:L20805
Wright JT. 2004. *Astron. J.* 128:1273–78
Yau KKC, Stephenson FR. 1988. *Q. J. R. Astron. Soc.* 29:175–97
Yu FL, Zong YQ, Lloyd JM, Leng MJ, Switzer AD, et al. 2012. *Holocene* 22:705–15
Zakharov V, Gandorfer A, Solanki SK, Löfdahl M. 2007. *Astron. Astrophys.* 461:695–95
Zhang Q, Soon WH, Baliunas SL, Lockwood GW, Skiff BA, Radick RR. 1994. *Ap. J. Lett.* 427:L111–14
Zwaan C. 1978. *Sol. Phys.* 60:213–40

Annual Review of Astronomy and Astrophysics

Volume 51, 2013

Contents